WORKING paper

BANQUE DE FRANCE
EUROSYSTÈME

The Sources of Global Supply Chain Tensions[1]

Moaz Elsayed, Christoph Grosse-Steffen and Magali Marx[2]

December 2025, WP 1026

Abstract

Why do only some supply-chain tensions generate persistent inflation, whereas others have more transitory effects? We decompose supply-chain tensions empirically into transportation and input-production shocks, while accounting for congestion. Both shocks lengthen supplier delivery times, showing that this common indicator can mask distinct structural sources of supply-chain tensions. Both are contractionary and inflationary, but input-production shocks generate more persistent effects on inventories, economic activity, and inflation, with a more persistent monetary-policy response. The macroeconomic consequences of supply-chain tensions therefore depend not only on their intensity, but also on their underlying source, with implications for the associated policy trade-offs. The structural historical decomposition yields monthly source-specific indicators covering 1969-2025.

Keywords: Global Supply Chains, Transportation Shocks, Input-production Shocks, Structural Vector Autoregressions, Inflation Persistence, Monetary Policy, Congestion.

JEL classification : C32, E31, E52, F60, R40

[1] We thank Guido Ascari, Christiane Baumeister, Fabrice Collard, Marco Del Negro, Francesco Del Prato, Valère Fourel, Mishel Ghassibe, Domenico Giannone, Callum Jones, Diego Känzig, Stéphane Lhuissier, Kristoffer Nimark, Lise Patureau, Gert Peersman, Franck Portier, Francesco Zanetti, Tao Zha and seminar participants at the Banque de France-TSE conference on *Unbalanced Sectoral Inflation Dynamics* (2023), Boston College, the Federal Reserve Bank of Boston, Mines Paris-PSL, Toulouse School of Economics, University of Helsinki, University of Bologna, Politecnico di Milano, 16th RCEA Bayesian Econometrics Workshop 2026, IAAE Annual Conference 2023, EEA-ESEM Congress 2023, Society for Computational Economics Conference 2023, AFSE Annual Congress 2023, for valuable comments that substantially improved the paper. An earlier version of this paper circulated under the title *Global Sectoral Supply Shocks, Inflation, and Monetary Policy*.

[2] moaz.elsayed@banque-france.fr, christoph.grossesteffen@banque-france.fr, magali.marx@banque-france.fr

NON-TECHNICAL SUMMARY

Global supply-chain disruptions have become a central concern for policymakers, as the Covid-19 pandemic and disruptions to maritime shipping routes have shown how sectoral shortages can propagate through production networks and affect activity and inflation. Yet an important question remains: which supply-chain disruptions generate persistent inflationary pressures? Common indicators such as supplier delivery times and shipping costs are useful for tracking supply-chain stress, but provide limited information about its underlying sources. Similar movements in these indicators may reflect economically distinct disturbances, with potentially different macroeconomic consequences.

We distinguish three sources of global supply-chain tensions within a common empirical framework. Transportation shocks disrupt logistics and shipping capacity, while input-production shocks reduce the availability of difficult-to-substitute intermediate inputs; a third shock captures congestion associated primarily with expansions in global activity. The key distinction between the two adverse supply shocks comes from transportation costs: both lengthen supplier delivery times and reduce economic activity, but transportation disruptions raise freight costs, whereas input-production disruptions lower them as weaker production reduces demand for transportation services. This allows us to identify the source, rather than only the intensity, of observed supply-chain tensions.

Figure 1.

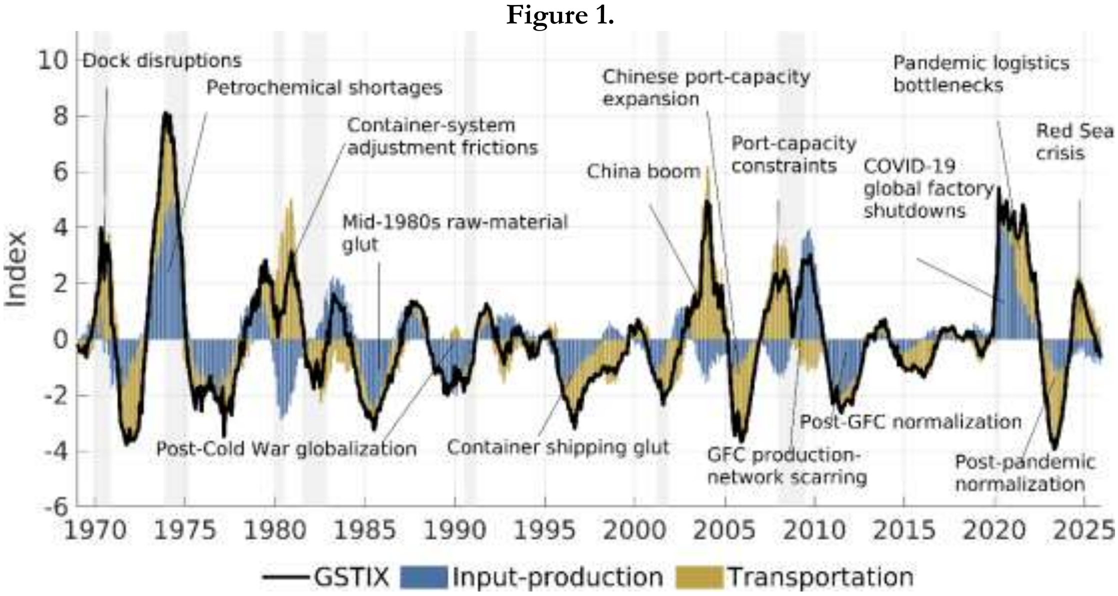

Note: Vertical grey bars denote NBER U.S. recessions. Positive values indicate above-average global supply-chain tensions, while negative values indicate below-average tensions. Black line reports the composite Global Supply Chain Tension Index (GSTIX), obtained by summing the standardized historical contributions of transportation and input-production shocks to the supplier-delivery-times index and real transportation costs. Blue and yellow areas provide a decomposition into the contributions of transportation and input-production tensions. Labels highlight selected historical episodes that illustrate the dominant source of supply-chain tensions. ***Source:*** Authors' calculations. The series is updated regularly and is publicly available at the Banque de France data portal Webstat.

Using this structural decomposition, we construct the Global Supply Chain Tension Index (GSTIX), a monthly measure of supply-side tensions covering 1969–2025. GSTIX separates transportation from input-production tensions and captures the dynamic effects of both current and past disruptions. Positive values indicate above-average tensions, while negative values capture periods of easing as adverse disruptions unwind. The index can therefore track not only the build-up of supply-chain stress but also its persistence and normalization over time. GSTIX is regularly updated and publicly available through the Banque de France data portal.

Figure 1 summarizes the historical evolution and changing composition of global supply-chain tensions over more than five decades. The decomposition identifies numerous episodes of tightening and easing, with substantial variation in the relative importance of transportation and input-production tensions. A few examples illustrate these patterns. During the rapid expansion of global trade in 2003–04, associated in part with China's integration into the world economy, transportation tensions increased as trade pressed against available shipping capacity, while input-production tensions eased as global manufacturing capacity expanded. The pandemic shows a different sequence: input-production tensions initially dominated amid factory closures and shortages of intermediate inputs, before transportation bottlenecks became increasingly important as production and trade recovered. The subsequent normalization of global supply chains appears as a pronounced easing of supply-side tensions, followed more recently by renewed transportation tensions during the Red Sea crisis. These episodes illustrate how similar levels of overall supply-chain stress can conceal very different—and changing—underlying sources.

To assess the macroeconomic consequences of these global shocks, we feed the identified transportation and input-production disturbances into a second-step model of the U.S. economy covering activity, inventories, prices, labor-market conditions, and the one-year Treasury yield. Both shocks are contractionary and inflationary, but their persistence differs markedly: transportation disruptions resemble a comparatively transitory cost-push shock, whereas input-production disruptions generate more persistent effects on inventories, economic activity, unemployment, consumer prices, and the monetary-policy response. The pandemic illustrates this distinction: transportation-related inflationary pressures faded as logistics normalized, while input-production disruptions remained inflationary for longer. The broader lesson is that the intensity of observed supply-chain stress is not sufficient for assessing its macroeconomic consequences: its source matters.

Les sources des tensions sur les chaînes d'approvisionnement mondiales

Résumé

Pourquoi certaines tensions sur les chaînes d'approvisionnement entraînent-elles une inflation persistante, tandis que d'autres ont des effets plus transitoires ? Nous décomposons empiriquement ces tensions en chocs liés au transport et en chocs liés aux intrants de production, tout en tenant compte des effets de congestion. Ces deux types de chocs allongent les délais de livraison des fournisseurs, ce qui montre que cet indicateur couramment utilisé peut masquer des sources structurelles distinctes de tensions sur les chaînes d'approvisionnement. Tous deux sont récessifs et inflationnistes, mais les chocs liés aux intrants de production génèrent des effets plus persistants sur les stocks, l'activité économique et l'inflation, ainsi qu'une réponse plus persistante de la politique monétaire. La source des tensions sur les chaînes d'approvisionnement joue donc un rôle déterminant dans leur propagation macroéconomique et les arbitrages de politique économique qui en découlent. La décomposition historique structurelle fournit des indicateurs mensuels propres à chaque source couvrant la période 1969-2025.

Mots clés : chaînes d'approvisionnement, chocs de transports, chocs de production des intrants, modèles vectoriels autorégressifs structurels, persistance de l'inflation, politique monétaire, congestion.

1 Introduction

Global supply-chain disruptions have become a central concern for policymakers. Episodes such as the Covid-19 pandemic and major disruptions to maritime shipping routes have highlighted how shortages originating in specific sectors can propagate through production networks and affect economic activity and inflation (Comin et al., 2023; Bai et al., 2026). Yet an important question remains unresolved: which supply-chain disruptions generate persistent inflationary pressures?

A common approach is to measure supply-chain tensions using indicators such as supplier delivery times, shipping costs, or composite indices of supply-chain pressures (e.g. Benigno et al., 2022). These indicators are useful for tracking disruptions in real time, but they provide limited information about the underlying sources of the observed stress. Our approach addresses this limitation by distinguishing the structural sources of observed supply-chain tensions. Two distinctions organize our analysis. First, we distinguish between supply-side disruptions originating in transportation services and in the production of intermediate inputs. Second, we separate these adverse supply disturbances from congestion associated with stronger global activity. As a result, similar movements in commonly used indicators can reflect transportation shocks, input-production shocks, or congestion, with potentially very different implications for macroeconomic dynamics.

We propose a parsimonious structural vector autoregression (SVAR) that treats transportation costs and supplier delivery times as endogenous equilibrium outcomes and identifies the disturbances that generate their joint movements. The model focuses on three variables that characterize global supply chains—transportation costs, supplier delivery times, and global industrial production—while keeping robust inference over the set of admissible structural models feasible. Transportation shocks disrupt logistics and shipping capacity and impede the movement of goods across locations, whereas input-production shocks disrupt the production of intermediate inputs that are difficult to substitute within production networks. Congestion shocks capture expansions in global activity relative to available transportation and input capacity. While both supply-side disturbances can generate shortages, lengthen supplier delivery times, and reduce economic activity, we document that they differ fundamentally in their propagation through the economy.

Our identification strategy exploits a differential implication for transportation costs. Transportation shocks raise transportation costs because they directly constrain the supply of logistics services or increase transportation demand through rerouting and substitution toward more costly shipping modes. Input-production shocks have the opposite implication for transportation costs. By reducing production activity and demand for complementary transportation services, they lower transportation costs even as delivery times lengthen. We document the plausibility of this central assumption for our identification approach in an illustrative production-network model with short-run rigidities in transportation supply. We use these opposite impact responses of transportation costs, together with narrative information and economically motivated bounds on selected contemporaneous coefficients, to identify the structural disturbances. Inference accounts for the multiplicity of structural models consistent with these restrictions using the robust Bayesian framework of Giacomini and Kitagawa (2021) and Giacomini et al. (2023).

Having identified the global shocks in this parsimonious system, we use them for two purposes. First, we construct the Global Supply Chain Tension Index (GSTIX), a monthly model-based decomposition of supply-side tensions in global supply chains from 1969 to 2025. GSTIX combines standardized historical contributions of transportation and input-production shocks to the supplier-delivery-times index and real transportation costs, and therefore summarizes both current disturbances and the propagation of past shocks. Second, we trace the identified global shocks through a larger system of U.S. macroeconomic variables, including activity, inventories, prices, labor-market conditions, and the one-year Treasury yield. Treating the global supply-chain block as exogenous to the U.S. economy allows us to study the conditional domestic propagation of the global shocks without requiring structural identification of the additional U.S. disturbances.

Our analysis delivers three main findings. First, transportation and input-production shocks account for a substantial share of fluctuations in supplier delivery time and real transportation cost over the business cycle. The historical evolution of the GSTIX composite index and its decomposition into transportation and input-production aligns closely with well-known disruption episodes and provides new insights into the sources of major supply-chain events since the 1970s. In particular, it reveals substantial variation in the relative importance of transportation disruptions and upstream input shortages across episodes that are often grouped together under the broad label of supply-chain stress.

Second, the two disturbances have markedly different macroeconomic consequences in U.S. data. By construction, both adverse supply shocks lengthen supplier delivery times and reduce global industrial production on impact, while their subsequent dynamics are unrestricted. Importantly, we impose no sign restrictions on U.S. activity, prices, labor-market variables, or interest rates. In U.S. data, both shocks are associated with weaker activity and higher price levels, but their effects differ sharply in persistence: input-production shocks generate more persistent responses than transportation shocks. The one-year Treasury yield also rises more persistently after input-production shocks. These results suggest that the source of observed supply-chain stress contains information about the likely persistence of its macroeconomic effects.

Third, we use our model to revisit the pandemic-era inflation surge. Global supply-chain tensions contributed materially to U.S. PCE inflation, but their relative contributions changed over time. Transportation and input-production shocks each contributed about 1.7 percentage points in 2021. In 2022, input-production shocks accounted for a larger share of the adverse supply contribution, while transportation-related contributions subsequently turned disinflationary as logistics conditions normalized. Input-production contributions remained positive for longer. This evolution suggests that the persistence of supply-chain related inflationary pressures depended not only on the overall magnitude of supply-chain stress, but also on the composition of the underlying disturbances. This distinction is consequential for real-time policy assessment: an easing of transportation bottlenecks need not imply that supply-chain-induced inflationary pressures have dissipated if more persistent input-production shortages remain in place.

Our paper contributes, first, to the empirical literature that measures and identifies global supply-chain disturbances. Benigno et al. (2022) develop the Global Supply Chain Pressure Index, which combines transportation costs and survey-based measures of supply-chain conditions into a comprehensive measure of global pressures, while explicitly seeking to purge its underlying series of demand effects. Using exceptionally rich vessel-level data, Bai et al. (2026) develop a novel measure of global port congestion based on the movements of containerships across major ports worldwide. Text-based approaches offer a complementary perspective: Burriel et al. (2024) construct a newspaper-based index that captures supply bottlenecks associated with events such as wars, natural disasters, and strikes, while Caldara et al. (2025) use an extensive corpus of newspaper articles to measure shortages of industrial goods, energy, food, and labor back to 1900. Our approach differs in its objective. We use structural identification to decompose observed supply-chain tensions into three economic sources: disruptions to transportation services, disruptions to input production, and congestion associated primarily with expansions in global activity. The decomposition therefore separates disturbances that can generate similar movements in commonly monitored supply-chain indicators but have different macroeconomic consequences.

Second, we add to the literature on the propagation of shocks through production networks. Microeconomic evidence shows that supplier disruptions can propagate widely through input-output linkages, with stronger effects when affected inputs or relationships are difficult to substitute in the short run (Barrot and Sauvagnat, 2016;

Boehm et al., 2019; Carvalho et al., 2021; Dhyne et al., 2021). This evidence motivates our interpretation of input-production disturbances as shocks whose effects can be amplified through production networks. The differential response of transportation costs used for identification is instead rationalized by the stylized model, which combines input complementarity with limited short-run adjustment of transportation capacity (Brancaccio et al., 2025a). We complement the microeconomic literature by identifying recurring global disturbances and tracing their aggregate propagation over a long historical sample.

Third, our findings relate to work on inflation dynamics in production networks. Sectoral disturbances can generate different inflation dynamics depending on their position in the network and on the interaction between input-output linkages and price rigidities (Afrouzi and Bhattarai, 2023; Rubbo, 2023). Nakov and Ghassibe (2025), in particular, show how upstream supply disturbances can generate persistent inflation through pricing cascades. Our empirical results are consistent with the broader implication that the propagation of a supply disturbance depends on where and how it enters the production network. We do not, however, directly identify the network position of the input-production shocks; rather, we find that the disturbances captured by our input-production classification are associated with more persistent U.S. price-level responses than transportation shocks.

Fourth, the paper speaks to the literature quantifying the drivers of the post-pandemic inflation surge. There is mounting evidence that supply-chain constraints and bottlenecks contributed materially to U.S. inflation during 2021–2022 (di Giovanni et al., 2022; Comin et al., 2023), while other studies emphasize the roles of sectoral demand composition (Ferrante et al., 2023), strong aggregate demand combined with accommodative policy (Bernanke and Blanchard, 2025; Giannone and Primiceri, 2024; Bocola et al., 2024), or amplification through labor-market tightness (Benigno and Eggertsson, 2023). We contribute to this debate in two ways. First, we separate adverse supply-chain disruptions from activity-induced congestion. Second, our quantitative decomposition helps reconcile evidence that supply-chain pressures mattered materially for post-pandemic inflation while showing that their macroeconomic implications depended critically on the underlying source.

Finally, our paper contributes to the empirical literature on set-identified SVARs. We apply the robust Bayesian framework of Giacomini et al. (2023) in a specification that combines contemporaneous sign restrictions, narrative restrictions on historical shock realizations, and inequality restrictions on selected contemporaneous coefficients, following the boundary-restriction logic of Kilian and Murphy (2012). These restrictions provide distinct identifying information: narrative restrictions discipline the interpretation of selected historical innovations, whereas boundary restrictions narrow economically implausible regions of the contemporaneous parameter space. Their combination substantially narrows the set of admissible structural models in our application.

The remainder of the paper is organized as follows. Section 2 presents the empirical model, data and identifying assumptions. Section 3 reports the baseline results, the construction of the source-specific supply-chain tension indicators, and robustness. Section 4 examines the propagation of the identified global shocks to the U.S. economy. Section 5 concludes.

2 Empirical model and identification

This section sets up the empirical model and establishes identification. To this end, it presents three sets of identifying assumptions: contemporaneous sign-restrictions, narrative restrictions on selected historical shock realizations, and economically motivated bounds on selected contemporaneous impact coefficients. We conduct inference using the robust Bayesian framework for set-identified models developed by Giacomini and Kitagawa (2021) and extended to narrative restrictions by Giacomini et al. (2023).

2.1 Model setup and data

We estimate a reduced-form vector autoregression (VAR) of the form

$$\boldsymbol{y}_t = \boldsymbol{B}\boldsymbol{x}_t + \boldsymbol{u}_t, \qquad \boldsymbol{u}_t \sim \mathcal{N}(\boldsymbol{0}, \boldsymbol{\Sigma}_u), \quad t = 1, \ldots, T, \tag{1}$$

where $\boldsymbol{y}_t$ is an $n \times 1$ vector of endogenous variables and $\boldsymbol{x}_t = (\boldsymbol{y}'_{t-1}, \ldots, \boldsymbol{y}'_{t-p}, 1, t)'$ contains p lags of the endogenous variables, a constant, and a linear time trend. The matrix $\boldsymbol{B}$ collects the corresponding reduced-form coefficients and $\boldsymbol{\Sigma}_u$ denotes the covariance matrix of the reduced-form innovations.

Data. We set $\boldsymbol{y}_t = (s_t, z_t, g_t)'$ to be a vector containing a measure of transportation cost (s_t), supplier delivery time (z_t), and world industrial production (g_t). Throughout, we take the logarithm of s_t, z_t enters in levels, and g_t enters in first differences of the logarithm. Transportation costs are expressed in real terms from a large cross-section of shipping and air freight indices, extending a measure proposed by Kilian (2009). Appendix B.2 provides a detailed explanation of the construction of the transportation cost index. Supplier delivery times are based on the global manufacturing PMI supplier delivery times, henceforth SDT. It is a monthly diffusion index based on survey responses among purchasing managers and tracks changes in the expected speed of supplier delivery. Values above 50 indicate slower delivery, while values below 50 indicate faster delivery. The information contained in the data is used by practitioners to decide when to place orders to prevent running out of inventories. We back-cast the global series prior to January 1998 using the corresponding supplier-delivery-time series on the U.S. economy from the Institute of Supply Management. Finally, global industrial production corresponds to the monthly industrial production of OECD countries plus six major emerging market economies following Baumeister and Hamilton (2019).

All data sources and transformations are described in Appendix B.1. In the baseline sample runs from January 1968 to December 2025, with the start date determined by the availability of the transportation cost series. We use 12 monthly lags and a linear time trend in the baseline specification.

2.2 Robust Bayesian identification

We follow the robust Bayesian identification framework of Giacomini and Kitagawa (2021) and Giacomini et al. (2023). Let $\boldsymbol{\Sigma}_{tr}$ denote the lower-triangular Cholesky factor of the reduced-form covariance matrix, such that $\boldsymbol{\Sigma}_u = \boldsymbol{\Sigma}_{tr}\boldsymbol{\Sigma}_{tr}'$. The reduced-form VAR in (1) can then be written in orthogonal-reduced form as

$$\boldsymbol{y}_t = \boldsymbol{B}\boldsymbol{x}_t + \boldsymbol{\Sigma}_{tr}\boldsymbol{Q}\boldsymbol{\varepsilon}_t, \qquad E(\boldsymbol{\varepsilon}_t\boldsymbol{\varepsilon}_t') = \boldsymbol{I}_n, \tag{2}$$

where $\boldsymbol{Q}$ is an $n \times n$ orthogonal matrix satisfying $\boldsymbol{Q}\boldsymbol{Q}' = \boldsymbol{I}_n$. Conditional on the reduced-form parameters $\boldsymbol{\phi} = (\boldsymbol{B}, \boldsymbol{\Sigma}_u)$, different values of $\boldsymbol{Q}$ represent observationally equivalent structural parameterizations. The structural shocks associated with a candidate rotation are

$$\boldsymbol{\varepsilon}_t = \boldsymbol{Q}'\boldsymbol{\Sigma}_{tr}^{-1}\boldsymbol{u}_t. \tag{3}$$

Our identifying restrictions constrain $\boldsymbol{Q}$ but do not point-identify it, leaving a set-identified SVAR (Rubio-Ramírez et al., 2010). Standard Bayesian inference therefore requires a conditional prior over observationally equivalent rotations that is not updated by the data and may affect posterior inference for economically relevant objects (Baumeister and Hamilton, 2015; Giacomini and Kitagawa, 2021). We instead follow the robust Bayesian approach of Giacomini and Kitagawa (2021); Giacomini et al. (2023), which reports inference that is uniform over the maintained class of such unrevisable conditional priors.

Let $\mathcal{R}$ denote the collection of identifying restrictions. We consider sign restrictions (SR) on contemporaneous impulse responses, narrative restrictions (NR) on structural shocks during selected historical episodes, and boundary restrictions (BR) on economically interpretable contemporaneous structural coefficients, following Kilian and Murphy (2012). Depending on the analysis, $\mathcal{R}$ denotes a particular combination of these restrictions, with $\mathcal{R}^{SR+NR+BR}$ serving as our baseline specification.

For a given reduced-form draw $\boldsymbol{\phi}$ and candidate rotation $\boldsymbol{Q}$, define the admissibility indicator

$$\mathcal{A}(\mathcal{R};\boldsymbol{\phi},\boldsymbol{Q}) = \mathbf{1}\left\{\boldsymbol{Q} \in \mathscr{Q}(\boldsymbol{\phi} \mid \mathcal{R}, \boldsymbol{Y}^T)\right\}, \tag{4}$$

where $\mathscr{Q}(\boldsymbol{\phi} \mid \mathcal{R}, \boldsymbol{Y}^T)$ denotes the set of orthogonal rotations satisfying all restrictions in $\mathcal{R}$. Sign and boundary restrictions constrain functions of the structural parameters and, conditional on $\boldsymbol{\phi}$, can be evaluated for each candidate rotation. Narrative restrictions additionally depend on the observed sample through the realized reduced-form innovations and the implied structural shocks. Hence, whenever $\mathcal{R}$ contains NR, the admissible set is data-dependent, as in Giacomini et al. (2023).

Our implementation extends the admissibility criterion used by Giacomini et al. (2023) with boundary restrictions. Algorithmically, the boundary restrictions enter as additional inequality checks on the contemporaneous coefficients implied by each candidate rotation. They do not otherwise alter the robust Bayesian procedure. A rotation is retained only if it jointly satisfies all restrictions in $\mathcal{R}$.

The distinction between data-independent and data-dependent restrictions matters for Bayesian inference. Following Giacomini and Kitagawa (2021); Giacomini et al. (2023), we consider the class of conditional priors for $\boldsymbol{Q}$ whose support is consistent with the sign and boundary restrictions. Because narrative restrictions depend on the realized data, they cannot be imposed through this conditional prior. Instead, they enter through the unconditional likelihood and truncate posterior support to rotations that also satisfy the narrative restrictions. Applying Bayes' rule to each admissible conditional prior therefore generates a class of posterior distributions for objects of interest, making inference robust to the choice of the unrevisable conditional prior over observationally equivalent structural parameterizations.

For scalar objects, we summarize this class of posterior distributions using the minimum-volume robust credible regions of Giacomini and Kitagawa (2021). A region with credibility α is required to contain posterior probability of at least α uniformly over the admissible posterior class, and we select the minimum-volume interval satisfying this requirement. Following Giacomini et al. (2023), we approximate these regions using the extrema of each scalar object over admissible rotations for every reduced-form draw. We report 68% and 90% robust credible regions; for impulse responses and FEVDs, they are constructed pointwise by horizon.

The reduced-form parameters are sampled from the conjugate diffuse posterior implied by a flat prior on $\boldsymbol{B}$ and a Jeffreys prior on $\boldsymbol{\Sigma}_u$, truncated to stable VARs. For the baseline specification, we retain 1,000 reduced-form posterior draws for which the complete collection of restrictions $\mathcal{R}^{SR+NR+BR}$ admits at least one rotation. This number describes the numerical sample used for the reported results and should be distinguished from a separate Monte Carlo convergence assessment.

Section 2.3 presents the identifying assumptions in detail, while Section 2.4 examines how the different layers of restrictions affect the posterior parameter distributions.

2.3 Identifying assumptions

This section presents the three sets of identifying assumptions by revisiting all sign restrictions, narrative restrictions, and boundary restrictions.

2.3.1 Sign restrictions

Sign Restriction 1: [transportation shock] *A transportation shock lowers global industrial production and increases supplier delivery time and transportation cost on impact.*

A negative global transportation supply shock (henceforth *transportation shock*) is an adverse disturbance to the supply of transportation services that reduces the effective capacity to move goods through global supply chains. Such disturbances may arise from physical disruptions to shipping routes or transport infrastructure, labor disputes, extreme weather and natural disasters, or other events that constrain available logistics capacity within a time-horizon that does not allow supply of transportation capacity to respond. We identify these disturbances by requiring them to raise transportation costs and supplier delivery times while lowering global industrial production on impact. Examples include port closures, disruptions to major shipping routes, strikes in the transportation sector, and failures of critical transport infrastructure.

Sign Restriction 2: [input-production shock] *An input-production shock lowers global industrial production, raises supplier delivery time, and lowers transportation cost on impact.*

A negative input-production supply shock (henceforth *input-production shock*) is an adverse disturbance to the supply of intermediate or final goods that reduces their availability to downstream producers. Such disturbances may arise from natural disasters, labor strikes, power outages, production failures, or restrictions on exports of critical inputs. Their effects can propagate through production networks when disrupted inputs are difficult to substitute, or require a time-consuming re-organization of firm relationships, thereby impairing production beyond the directly affected firms or sectors (Acemoglu et al., 2012). We identify these disturbances by requiring them to lower transportation costs, raise supplier delivery times, and lower global industrial production on impact. The latter restriction reflects the complementarity between goods production and transportation services: lower production reduces the demand for transportation, placing downward pressure on transportation prices. This effect can be particularly pronounced when transportation supply is inelastic in the short run.[1]

Sign Restriction 3: **[congestion shock]** *A congestion shock increases global industrial production, transportation cost, and supplier delivery time on impact.*

We refer to the third disturbance as a *congestion shock*. It captures an expansion in global activity relative to available transportation capacity and input availability, thereby increasing the utilization of global supply chains. While such congestion is primarily associated with demand-driven expansions, we allow for a broader interpretation. For example, exogenous technological shifts that raise production without proportionate expansions in transportation capacity or input availability may generate similar pressures. We identify these disturbances by requiring them to raise global industrial production, transportation costs, and supplier delivery times on impact.

Model-based rationale. A stylized static rationale for the impact sign patterns associated with the two adverse supply shocks is presented in Appendix A. The model contains a stylized production chain that combines limited short-run adjustment of transportation capacity with complementarity between transportation services and intermediate inputs. The global-activity sign pattern is interpreted through a congestion mechanism: stronger activity raises the demand for freight and increases pressure on existing production and logistics capacity. The appendix is intended to rationalize these contemporaneous signs rather than the dynamic persistence estimated in the SVAR.

Combining restrictions 1–3, we impose sign restrictions on the contemporaneous impact matrix $\boldsymbol{\Sigma}_{tr}\boldsymbol{Q}$. Rows correspond to transportation cost, supplier delivery time, and global industrial production, while columns correspond to the transportation, input-production, and congestion shocks. Tab. 1 summarizes the resulting restrictions.

[1] Brancaccio et al. (2025b) show that fluctuations in the demand for maritime transportation face a highly inelastic supply curve, reflecting equilibrium bottlenecks in both shipping capacity and port infrastructure, and therefore translate into large movements in shipping prices.

Table 1: Sign restrictions on contemporaneous responses

	Transportation shock	Input-production shock	Congestion shock
Transportation cost	+	−	+
Supplier delivery time	+	+	+
Global industrial production	−	−	+

2.3.2 Narrative restrictions

We refine identification using narrative restrictions on the sign of selected structural innovations at historically informative dates, following the idea of narrative sign restrictions in Antolin-Diaz and Rubio-Ramirez (2018) and their robust-Bayesian implementation in Giacomini et al. (2023). The selected episodes provide information about whether the transportation or input-production component is likely to have been adverse in a given month; they do not imply that the other structural disturbances were zero. Tab. 2 lists the episodes used for identification in the baseline specification. Appendix D provides a detailed discussion of each episode.

Table 2: Episodes used for narrative sign restrictions

No.	**Event**	**Date**
Transportation shocks		
1	Great Hanshin earthquake (Kobe), Japan	January 1995
2	Hurricane Katrina, United States	September 2005
3	Eyjafjallajökull volcanic eruption, Iceland	April 2010
4	Hanjin Shipping bankruptcy, South Korea	September 2016
5	Suez Canal blockage, Egypt	March 2021
6	Panama canal drought, Panama	August 2023
7	Red Sea shipping attacks, Bab el-Mandeb Strait	November 2023
Input-production shocks		
8	Benguela Railway closure (copper-cobalt exports), Angola	August 1975
9	Second Shaba invasion (copper-cobalt), Zaire (DR Congo)	May 1978
10	Chi-Chi earthquake, Taiwan	September 1999
11	Wenchuan (Sichuan) earthquake, China	May 2008
12	Great East Japan earthquake and tsunami	March 2011
13	Thailand floods (Chao Phraya basin)	October 2011

Notes: Narrative sign restrictions are imposed only on impact (one month). Appendix D discusses the historical background and economic impact of each event. Robustness with respect to events is presented in Section 3.4.3.

The transportation episodes comprise natural disasters and logistical disruptions that temporarily impaired the movement of goods while leaving production capacity largely unaffected. They include major port closures (Kobe earthquake, Hurricane Katrina), disruptions to air transportation (Eyjafjallajökull eruption), shipping-market disturbances (Hanjin Shipping bankruptcy), and blockages to maritime choke points (Suez Canal blockage, Panama Canal drought, and Red Sea shipping attacks). Each episode generated substantial interruptions to international freight transportation.

The input-production episodes comprise events that disrupted the production or availability of key intermediate inputs while leaving transportation networks largely intact. They include interruptions to mineral supply (Benguela Railway closure and the Second Shaba invasion) and major natural disasters affecting manufacturing hubs (Chi-Chi earthquake, Wenchuan earthquake, Great East Japan earthquake and tsunami, and Thailand floods). These events generated sizeable production shortfalls that propagated internationally through global supply chains.

Discussion. Our narrative restrictions are based on historical episodes that increased transportation frictions or disrupted input production. Accordingly, the identified shocks should be interpreted as adverse supply-chain disturbances. While this does not permit testing whether equivalent improvements would have symmetric effects, it is consistent with the paper's objective of identifying the macroeconomic consequences of supply-chain tensions. Moreover, comparable exogenous episodes leading to sudden improvements in global supply-chain conditions are largely absent from the historical record. Within this framework, some historical episodes admit more than one interpretation. The closure of the Benguela Railway illustrates this point. Although the disruption affected a transportation corridor, we classify it as an input-production shock because its principal economic consequence was a shortage of cobalt—a critical industrial input—rather than widespread disruptions to global transportation networks. To assess the sensitivity of both our classification decisions and the selected narrative episodes, Section 3.4.3 reports leave-one-event-out robustness exercises.

2.3.3 Boundary restrictions

Our third set of restrictions uses external economic information about selected contemporaneous relationships. To formulate these restrictions, we recover the simultaneous structural representation associated with each candidate rotation. Under the unit-variance normalization for structural shocks in (2), the contemporaneous coefficient matrix implied by a candidate rotation is

$$\widetilde{\boldsymbol{A}}_0 = \boldsymbol{Q}'\boldsymbol{\Sigma}_{tr}^{-1}.$$

We normalize each structural equation to have a unit coefficient on its own endogenous variable. Specifically, letting

$$\boldsymbol{D} = \operatorname{diag}\left(\widetilde{A}_{0,11}^{-1}, \widetilde{A}_{0,22}^{-1}, \widetilde{A}_{0,33}^{-1}\right),$$

the normalized contemporaneous coefficient matrix is $\boldsymbol{A}_0 = \boldsymbol{D}\widetilde{\boldsymbol{A}}_0$, which we write as

$$\boldsymbol{A}_0 = \begin{pmatrix} 1 & -\alpha_{sz} & -\alpha_{sg} \\ -\alpha_{zs} & 1 & -\alpha_{zg} \\ -\alpha_{gs} & -\alpha_{gz} & 1 \end{pmatrix}. \tag{5}$$

Under this normalization, the contemporaneous structural equations are

$$s_t = \alpha_{sz} z_t + \alpha_{sg} g_t + \gamma_1' \boldsymbol{x}_t + \varepsilon_{1t}, \tag{6}$$

$$z_t = \alpha_{zs} s_t + \alpha_{zg} g_t + \gamma_2' \boldsymbol{x}_t + \varepsilon_{2t}, \tag{7}$$

$$g_t = \alpha_{gs} s_t + \alpha_{gz} z_t + \gamma_3' \boldsymbol{x}_t + \varepsilon_{3t}. \tag{8}$$

The coefficients α_{ij} therefore describe partial contemporaneous relationships within the simultaneous system. γ_i collects the lag and deterministic coefficients of equation i. Under our identifying restrictions, ε_{1t}, ε_{2t}, and ε_{3t} correspond to the transportation, input-production, and congestion disturbances, respectively.

Equation (6) describes the contemporaneous determinants of transportation costs. The coefficient α_{sz} captures the partial relationship between the price and delivery-time dimensions of transportation services, while α_{sg} captures the effect of aggregate activity on transportation costs through transportation demand. Equation (7) summarizes the contemporaneous determinants of supplier delivery time: one determinant is transportation costs, through α_{zs}, and another is global activity, through α_{zg}. Finally, (8) allows global manufacturing activity to depend contemporaneously on transportation costs, through α_{gs}, and supplier delivery time, through α_{gz}.

Following the logic of Kilian and Murphy (2012), the boundary restrictions use external information to constrain selected coefficients of the normalized contemporaneous system rather than imposing exact exclusion restrictions. We impose admissible intervals on four contemporaneous response coefficients. Because the variables enter the VAR in different transformations, these coefficients have different units and should not all be interpreted as dimensionless elasticities. Tab. 3 summarizes the restrictions. Because the coefficients describe partial relationships within a simultaneous system, their signs need not coincide with unconditional comovements in the data.

Assumption BR1 imposes a weakly negative contemporaneous response of trans-

Table 3: Bounds on contemporaneous structural parameters

#BR	param.	description	bounds
Transportation-service market			
BR1	α_{sz}	transportation-cost response to supplier-delivery index	$[-\infty, 0]$
BR2	α_{sg}	transportation-cost response to output growth	$[0, 2]$
Production and supply-chain congestion			
BR3	α_{gs}	output-growth response to transportation costs	$[-\infty, 0]$
BR4	α_{zg}	supplier-delivery-index response to output growth	$[0, 3]$

Notes: The contemporaneous coefficients subject to boundary restrictions are expressed in the units implied by the transformation of the variables. α_{sz} measures the percent response of transportation costs to a one-index-point change in supplier delivery time; α_{sg} the percent response of transportation costs to a one-percentage-point change in monthly industrial-production growth; α_{gs} the percentage-point response of monthly industrial-production growth to a one-percentage-point change in transportation costs; and α_{zg} the index-point response of supplier delivery time to a one-percentage-point change in monthly industrial-production growth. The numerical bounds are therefore conditional on the scaling of the variables.

portation costs to supplier delivery time, $\alpha_{sz} \leq 0$. The restriction reflects the price–quality relationship in transportation services: faster and more reliable delivery constitutes a higher-quality service for which firms are willing to pay a premium. Accordingly, holding transportation demand, capacity conditions, and other cost determinants fixed, slower delivery should not command a higher transportation price. Hummels and Schaur (2013) formalize this trade-off through exporters' choice between fast but expensive air transport and slower but cheaper ocean transport. Using detailed U.S. import data, they estimate that an additional day in transit is equivalent to an ad valorem trade cost of 0.6–2.1 percent. In our SVAR, however, α_{sz} measures the percent response of transportation costs to a one-index-point increase in SDT rather than the cost associated with an additional day in transit. The estimates of Hummels and Schaur (2013) therefore discipline the sign of this relationship but do not provide a direct calibration of its magnitude. We consequently impose only the weak restriction $\alpha_{sz} \in [-\infty, 0]$.

Assumption BR2 restricts the contemporaneous response of transportation costs to output growth to the interval $\alpha_{sg} \in [0, 2]$. The positive lower bound reflects the derived demand for transportation services: stronger production increases freight demand and, for given transportation capacity, raises equilibrium transportation costs. Hamilton (2019) describes this supply-and-demand mechanism explicitly, noting that increases in global economic activity raise the demand and cost of shipping, whereas expansions in shipping capacity and productivity lower transportation prices. Fuchs and Wong (2026) formalize how capacity constraints and congestion amplify this price response in multimodal freight markets. In our SVAR α_{sg} measures the percent response of transportation costs to a one-percentage-point increase in monthly industrial-production growth. Since the literature does not provide a direct estimate of this aggregate contemporaneous response coefficient, we treat the upper bound of two as an economically motivated regularization rather than a calibrated estimate, ruling out implausibly large contemporaneous responses.

Assumption BR3 imposes a non-positive contemporaneous response of output growth to transportation costs, $\alpha_{gs} \in [-\infty, 0]$. Higher freight costs raise the cost of procuring intermediate inputs and distributing final goods and therefore reduce firms' incentives to produce. Closely related evidence is provided by Alessandria et al. (2023), who study transportation frictions arising from longer shipping and restocking times in a quantitative model with input-output linkages and inventory management. Higher shipping delays increase the effective cost of inputs and reduce production, with inventory depletion and stockouts amplifying the contractionary effects. In our SVAR α_{gs} measures the percentage-point response of monthly industrial-production growth to a one-percent increase in transportation costs. Since the available evidence supports the direction of the relationship but does not provide a direct estimate of this contemporaneous response coefficient, we impose only the inequality restriction $\alpha_{gs} \leq 0$.

Assumption BR4 restricts the contemporaneous response of supplier delivery time to output growth to the interval $\alpha_{zg} \in [0, 3]$. The positive lower bound reflects the well-established relationship between production utilization and lead times: as production rises relative to available capacity, congestion and production queues lengthen supplier delivery times. While this mechanism is established most directly at the firm level, it also applies to production networks, where higher activity raises capacity utilization and inventory adjustment and input linkages can propagate local bottlenecks across suppliers. In our SVAR α_{zg} measures the increase in the SDT index, in index points, associated with a one-percentage-point increase in monthly industrial-production growth. The upper bound of three is not implied by queueing theory itself, but reflects aggregation across firms with heterogeneous utilization rates and the mitigating role of supplier substitution and inventories. It therefore rules out implausibly large contemporaneous elasticities that would require economy-wide production to operate close to capacity simultaneously.

2.4 Posterior densities of contemporaneous elasticities

This section examines how the different collections of identifying restrictions shape the posterior densities of the contemporaneous model elasticities. Fig. 1 reports the densities of the six elasticities under $\mathcal{R}^{\text{SR+NR}}$, $\mathcal{R}^{\text{SR+BR}}$, and the baseline collection $\mathcal{R}^{\text{SR+NR+BR}}$. For each draw of the reduced-form parameters $\boldsymbol{\phi}$ and orthogonal rotation $\boldsymbol{Q}$, we recover the corresponding contemporaneous elasticities from the normalized structural coefficient matrix $\boldsymbol{A}_0$. A draw is retained whenever the admissibility criterion (4) is satisfied. The reported densities are constructed by pooling the elasticities implied by the retained draws under each collection of restrictions $\mathcal{R}$. They therefore describe the posterior distribution affected by the reference sampling scheme over admissible rotations. Unlike the robust credible regions reported below for impulse responses and forecast error variance decompositions, these densities are not robustified over the full class of admissible conditional priors for $\boldsymbol{Q} \mid \boldsymbol{\phi}$.

Figure 1: Posterior densities under alternative identifying assumptions

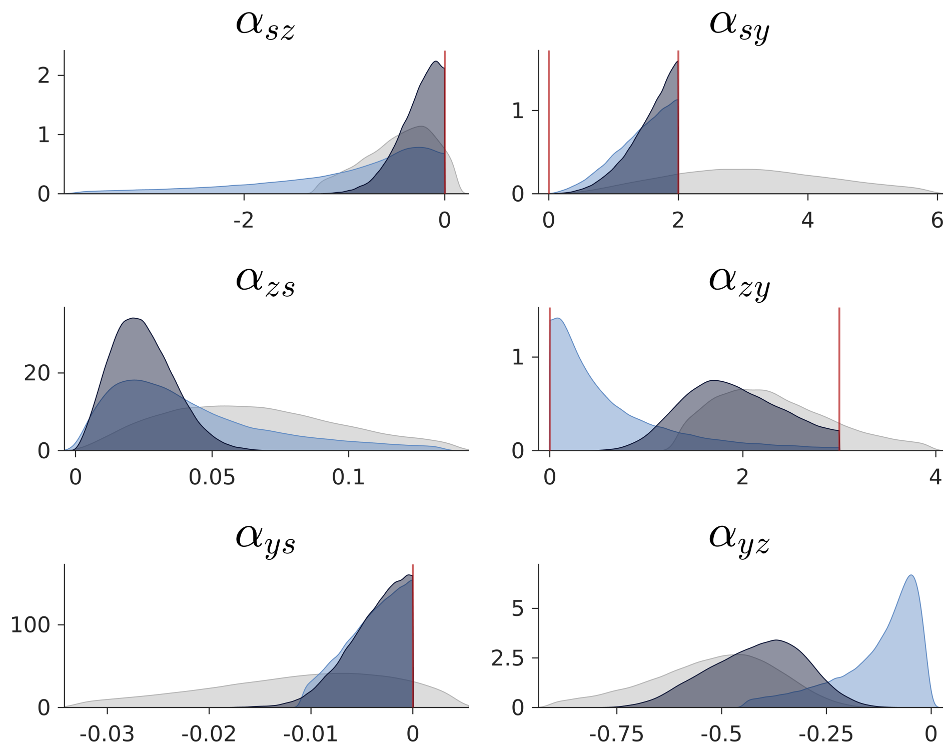

Notes: Dark blue = $\mathcal{R}^{\text{SR+NR+BR}}$ (baseline); blue = $\mathcal{R}^{\text{SR+BR}}$; grey = $\mathcal{R}^{\text{SR+NR}}$. Red vertical lines indicate BR interval bounds where applicable. For display, the $\mathcal{R}^{\text{SR+NR}}$ and $\mathcal{R}^{\text{SR+BR}}$ densities are trimmed as follows. For $\mathcal{R}^{\text{SR+NR}}$, unbounded sides are trimmed at the 5th or 95th percentile. For $\mathcal{R}^{\text{SR+BR}}$, no trimming is applied when both sides are bounded, while the single unbounded tail is trimmed at the 5th or 95th percentile when only one side is bounded. The baseline densities are shown without trimming.

Under sign and narrative restrictions alone, the sampled admissible coefficients remain relatively diffuse (Fig. 1, grey areas). The narrative restrictions discipline selected historical shock realizations but leave broad latitude for the contemporaneous mapping between shocks and observables. The remaining dispersion therefore reflects weak identification of those contemporaneous coefficients under this restriction set.

The boundary restrictions, imposed together with the sign restrictions in $\mathcal{R}^{\text{SR+BR}}$, affect the posterior distributions in a markedly different way (Fig. 1, blue areas). Relative to $\mathcal{R}^{\text{SR+NR}}$, they place posterior mass in substantially different regions of the admissible parameter space for several elasticities. The distinction is therefore not merely one of posterior concentration. Rather, the elasticity bounds contribute qualitatively different identifying information by directly constraining contemporaneous equilibrium relationships, whereas the narrative restrictions discriminate among structural models through the historical realizations of the shocks.

A substantial gain in identification arises when both sources of prior information are combined in the baseline collection with sign restrictions as $\mathcal{R}^{\text{SR+NR+BR}}$ (Fig. 1, dark areas). Narrative restrictions become more informative through historical episodes, since boundary restrictions rule out structural parameterizations that violate economically motivated bounds on the contemporaneous elasticities. While adding restrictions successively somewhat mechanically shrinks the admissible set of rotations, the meaningful complementarity between BR and NR for the identification of tensions in global supply chains is particularly visible for elasticities such as α_{sz} and α_{zs}.

3 Estimation results

This section presents the results based on the three variable structural VAR. In addition to more standard results on the dynamics, we compute novel measures of supply chain tensions based on the structurally identified model.

3.1 Impulse response analysis

Fig. 2 reports the responses of the three global variables to one-standard-deviation structural shocks. The dark and light bands denote the 68% and 90% pointwise robust credible regions, respectively. Transportation costs are expressed in percentage deviations, supplier delivery times in index points, and world industrial production in cumulative percentage deviations from the no-shock path.

A contractionary transportation-supply shock immediately raises transportation costs by approximately 8–10% (Fig. 2, top row). The response remains elevated during the first year, with the 68% robust credible region lying roughly between 5% and 9% at twelve months, before declining toward zero over the following year. Transportation costs temporarily fall below baseline after about two years, but the magnitude of this reversal is modest relative to the initial increase. Supplier delivery time rises by approximately 0.1–0.3 index points on impact and reaches a peak of about 0.3–0.6

points within the first year. The response subsequently reverses, reaching approximately -0.2 to -0.6 index points after two years, before returning toward zero. The cumulative response of world industrial production is initially close to zero but becomes increasingly negative as the disruption propagates. After roughly three years, the 68% robust credible region lies approximately between -0.6 and -0.2 percent, and the production level remains below baseline at the five-year horizon. Thus, transportation disruptions have large and relatively immediate effects on logistics prices and delivery performance, while their real effects emerge more gradually and persist beyond the direct transportation-market disruption.

Figure 2: Impulse responses

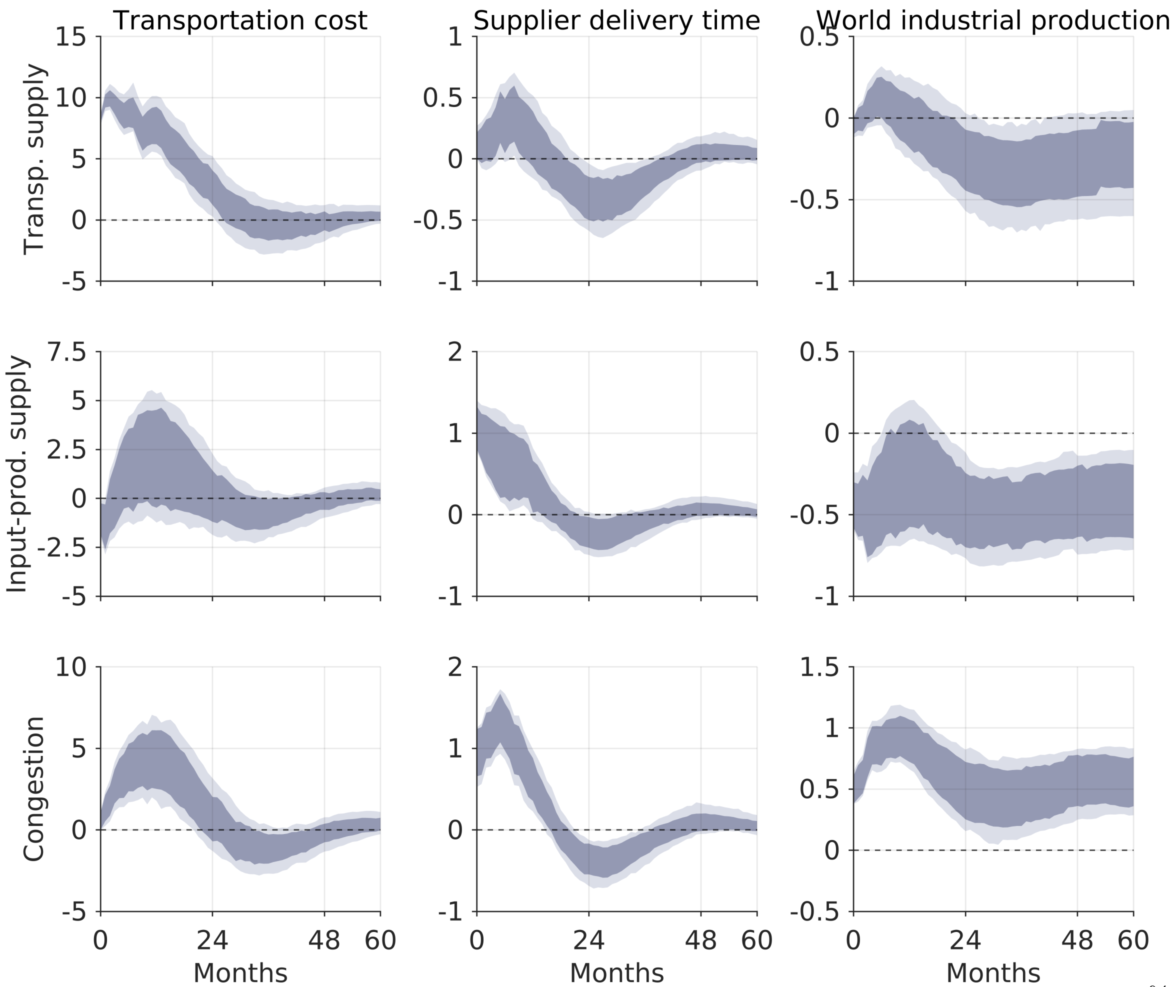

Notes: Responses to a one-standard-deviation structural shock. Dark and light bands denote 68% and 90% pointwise robust credible regions, respectively, following Giacomini et al. (2023), computed separately for each response and horizon. Columns report real transportation costs, supplier delivery time, and world industrial production; rows report transportation-supply, input-production, and congestion shocks. The baseline identification combines sign, narrative, and boundary restrictions. Transportation costs are measured in percentage deviations from the pre-shock level, supplier delivery time in index points, and world industrial production in cumulative percentage deviations.

An adverse input-production shock also increases supplier delivery times and depresses global activity, but it lowers transportation costs (Fig. 2, middle row). On impact, posterior mass of the transportation-cost response is clearly concentrated below zero, while the effect beyond the initial months is imprecisely estimated. Between roughly two and three years, the 68% region lies approximately between -1.5 and zero percent, after which the response gradually dissipates. Supplier delivery time rises sharply on impact, by approximately 0.8–1.2 index points, and remains positive during most of the first year. It subsequently falls below baseline, undershooting slightly after two years, before normalizing. The cumulative effect on world industrial production is negative throughout the reported horizon. The 68% region is approximately -0.6 to -0.2 percent after two to three years and remains near that range after five years. The combination of longer delivery times, weaker production, and comparatively low transportation costs distinguishes input-production shortages from disruptions originating in the transportation sector. It also shows that deteriorating supplier delivery times alone do not reveal the structural source of supply-chain tensions. The opposite response of transportation costs is a distinctive feature of input-production shocks. Much of the existing literature has provided important evidence on aggregate supply-chain or shipping disruptions characterized by joint increases in freight costs and delivery time. Our decomposition highlights a complementary configuration: upstream input shortages can lengthen delivery times while lowering freight demand and transportation cost.

A congestion shock raises transportation costs, supplier delivery times, and industrial production simultaneously (Fig. 2, bottom row). Transportation costs increase by roughly 1% on impact and peak after approximately one year, when the 68% credible region lies around 3–6%. The response then declines, crosses zero after about two years, and becomes mildly negative before returning toward baseline. Supplier delivery time rises by approximately 0.8–1.2 index points on impact and peaks within the first six months at around 1–1.5 points. The response then falls rapidly, becoming negative after roughly eighteen months and reaching around -0.6 to -0.2 points after two to three years. World industrial production rises on impact by approximately 0.5%, peaks at around 0.8–1.1% during the first year, and subsequently declines. Nevertheless, the cumulative response remains positive over the full five-year horizon, with the 68% robust credible region still approximately 0.3–0.7% at sixty months. This joint increase in activity, freight costs, and delivery times is consistent with demand-induced congestion: stronger production strains short-run transportation and input capacity, raising both logistics prices and delivery delays. Because the production response is cumulative and no long-run restriction is imposed, its persistent level effect should not by itself be interpreted as evidence of hysteresis. The joint increase in output, transportation costs, and delivery times is consistent with models in which stronger demand strains short-run production and logistics capacity (Comin et al., 2023).

Taken together, the responses reveal three distinct sources of observed supply-chain tensions. Transportation shocks generate large increases in freight costs followed by delayed output losses. Input-production shocks reduce output persistently while placing less upward pressure on transportation costs, reflecting weaker derived demand for freight services. Congestion shocks, by contrast, raise output, transportation costs, and delivery times jointly. The results therefore show that similar movements in supplier delivery times can arise from structural disturbances with sharply different implications for transportation prices and global activity.

3.2 Forecast error variance decomposition

Fig. 3 reports the forecast error variance decomposition of the three global variables under the baseline identification. The decomposition complements the impulse response analysis by quantifying the relative importance of each structural shock for fluctuations in the three global series over different forecast horizons. Three findings stand out.

First, transportation supply shocks account for the dominant share of fluctuations in transportation costs at all horizons. They explain almost the entire forecast error variance on impact and remain the dominant source of transportation-cost variation even after five years, with a contribution of roughly 60–80%. Congestion shocks become increasingly important at medium horizons, eventually accounting for approximately one quarter to one third of transportation-cost fluctuations, whereas input-production shocks contribute only modestly throughout. This decomposition supports the structural interpretation of the transportation shock as the primary driver of freight-price dynamics.

Second, supplier delivery time is largely driven by input-production and congestion shocks rather than transportation shocks. On impact, the forecast error variance is almost entirely explained by these two shocks, with each accounting for a substantial share of fluctuations. While the contribution of input-production shocks declines gradually over time, it remains economically important even after five years. Congestion shocks explain an equally persistent fraction of delivery-time fluctuations, whereas transportation supply shocks account for only a relatively small share throughout the forecast horizon, increasing only gradually to around 15%. This finding reinforces one of the central messages of the paper: Similar increases in supplier delivery times may originate from fundamentally different structural disturbances, including upstream production bottlenecks and congestion induced by strong global demand.

Figure 3: Forecast error variance decomposition

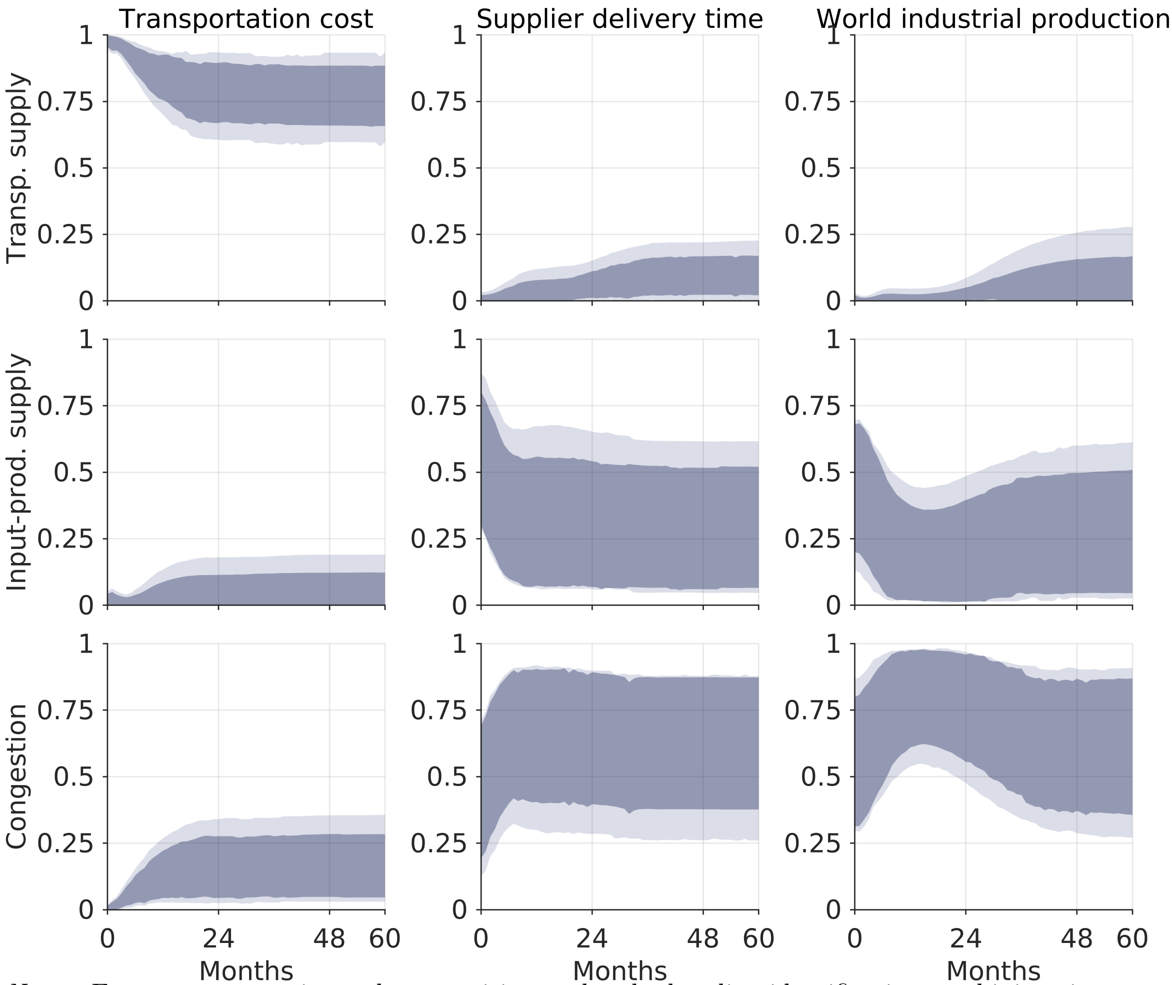

Notes: Forecast error variance decomposition under the baseline identification combining sign, narrative, and boundary restrictions. Rows correspond to structural shocks (transportation supply, input-production supply, and congestion), and columns to observable variables (transportation costs, supplier delivery time, and world industrial production). Entries report the share of the forecast error variance attributable to each structural shock at monthly horizons. For each variable and horizon, the three shares sum to one. Dark and light bands denote the 68% and 90% pointwise robust credible regions, respectively, following Giacomini et al. (2023), which are computed separately for each variable and horizon.

Third, fluctuations in world industrial production are primarily explained by congestion and input-production shocks, while transportation supply shocks play only a limited role. Congestion shocks dominate short-run output fluctuations, explaining approximately one third to three quarters of the forecast error variance on impact. At medium and longer horizons, however, the contribution of input-production shocks increases steadily, reaching roughly one quarter of the forecast error variance after five years. Transportation supply shocks account for only a comparatively small fraction of output fluctuations over the entire horizon. Thus, transportation disruptions have economically meaningful conditional effects, but account for only a small fraction of unconditional fluctuations in global industrial production. Persistent fluctuations in global activity instead primarily reflect upstream production disturbances and congestion effects.

Taken together, the FEVDs reinforce the interpretation of the two supply-side structural shocks. Transportation shocks dominate fluctuations in transportation costs, whereas supplier delivery times primarily reflect input-production and congestion shocks. Moreover, medium- and long-run fluctuations in global industrial production are explained mainly by input-production and congestion shocks.

3.3 Measuring source-specific global supply-chain tensions

The structural model allows us to summarize the historical intensity and sources of global supply-chain tensions. We use the SVAR's historical decomposition to attribute movements in transportation costs and supplier delivery times to current and past realizations of the structural shocks that generated them. The resulting indices distinguish supply-side tensions originating in transportation and input production from congestion associated primarily with expansions in global activity.

For each admissible structural model, we recover the historical contribution of each structural shock to transportation costs and the supplier-delivery-times index. Because these contributions are measured in different units, we standardize each shock-by-variable contribution over the historical sample before aggregation. This construction makes the components dimensionless and gives equal weight to the standardized transportation-cost and supplier-delivery dimensions for each structural source. The resulting index is therefore a model-based standardized measure of tension, not a quantity in physical units. Specifically, letting $HD_{j,t}^k$ denote the historical contribution of structural shock k to variable j in period t, we define

$$\widetilde{HD}_{j,t}^k = \frac{HD_{j,t}^k - \overline{HD}_j^k}{\sigma(HD_j^k)}, \qquad j \in \{s, z\},$$

where $\overline{HD}_j^k$ and $\sigma(HD_j^k)$ denote the time-series mean and standard deviation of the respective historical-contribution series. We define the *Global Supply Chain Tension Index* (GSTIX) as the sum of the standardized transportation- and input-production-shock contributions to these two variables,

$$\text{GSTIX}_t = \underbrace{\widetilde{HD}_{s,t}^{\text{TRNS}} + \widetilde{HD}_{z,t}^{\text{TRNS}}}_{\text{GSTIX}_t^{\text{TRNS}}} + \underbrace{\widetilde{HD}_{s,t}^{\text{INPT}} + \widetilde{HD}_{z,t}^{\text{INPT}}}_{\text{GSTIX}_t^{\text{INPT}}}.$$

Thus, $\mathrm{GSTIX}_t^{\mathrm{TRNS}}$ and $\mathrm{GSTIX}_t^{\mathrm{INPT}}$ measure source-specific supply-chain tensions, while their sum yields the composite supply-side index. The construction gives the two observable dimensions equal weight after standardization; the resulting GSTIX components and their composite are not themselves normalized to unit variance.

For each month, the historical decomposition expresses the observed realization of every endogenous variable as the sum of the dynamic contributions of current and past structural shocks.[2] At each date, the historical decomposition includes the dynamic effects of current and past shocks. An elevated index value may therefore reflect either a large recent disturbance or the continued propagation of earlier shocks. Combining the two standardized observables captures the joint price and delivery-condition manifestations of supply-chain stress. Positive values denote above-average supply-side tension under this normalization, whereas negative values denote below-average tension.

Panel (a) of Fig. 4 reports the composite GSTIX together with its robust credible region. The index identifies several major episodes of global supply-chain stress over the past five decades. Tensions rise sharply during the 1973–74 energy and raw-material crisis and again around the second oil shock in 1979–80. A further increase in 2003–04 coincides with the rapid expansion of global trade and mounting pressure on transportation capacity. Around the Global Financial Crisis, tensions initially rise but subsequently reverse as global trade and production contract sharply. The pandemic generates the largest sustained increase in recent decades, followed by a pronounced easing of supply-side tensions during the normalization of global supply chains in 2023–24. The prominence of the 1970s episodes partly reflects the broader supply-chain consequences of the energy crises. In 1973–74, for example, disruptions to energy and raw-material supplies cascaded into shortages of petrochemical feedstocks, plastics, and resins. Drawing on industry-level evidence and contemporaneous trade publications, Lee and Ni (2002) document that the oil shock impaired supply in petroleum refining and industrial chemicals, illustrating how energy disruptions propagated into shortages of intermediate inputs. Importantly, adding the real price of oil to the SVAR leaves the impulse responses to transportation and input-production shocks largely un-

[2] Let $\boldsymbol{\Psi}_h$ denote the reduced-form moving-average coefficient at horizon h and let $\boldsymbol{C}_h = \boldsymbol{\Psi}_h \boldsymbol{P}\boldsymbol{Q}$ denote the corresponding structural impulse-response matrix. Abstracting from deterministic terms and initial conditions, the historical contribution of shock k to variable j in period t is

$$HD_{j,t}^{k} = \sum_{h=0}^{t-1} \boldsymbol{e}_j' \boldsymbol{C}_h \boldsymbol{e}_k \epsilon_{k,t-h}^{*},$$

where $\boldsymbol{e}_j$ and $\boldsymbol{e}_k$ are selection vectors. At date t, the decomposition includes all shock realizations since the beginning of the effective sample through the corresponding moving-average coefficients; no fixed truncation horizon is imposed.

Figure 4: Historical sources of global supply-chain tensions

(a) The composite Global Supply Chain Tension Index (GSTIX)

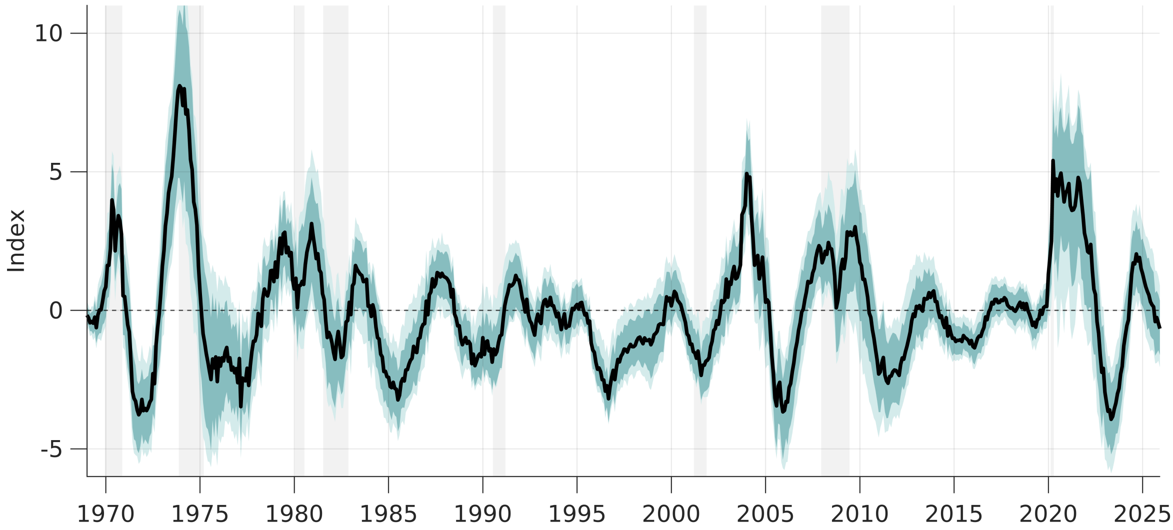

(b) GSTIX decomposition into transportation and input-production

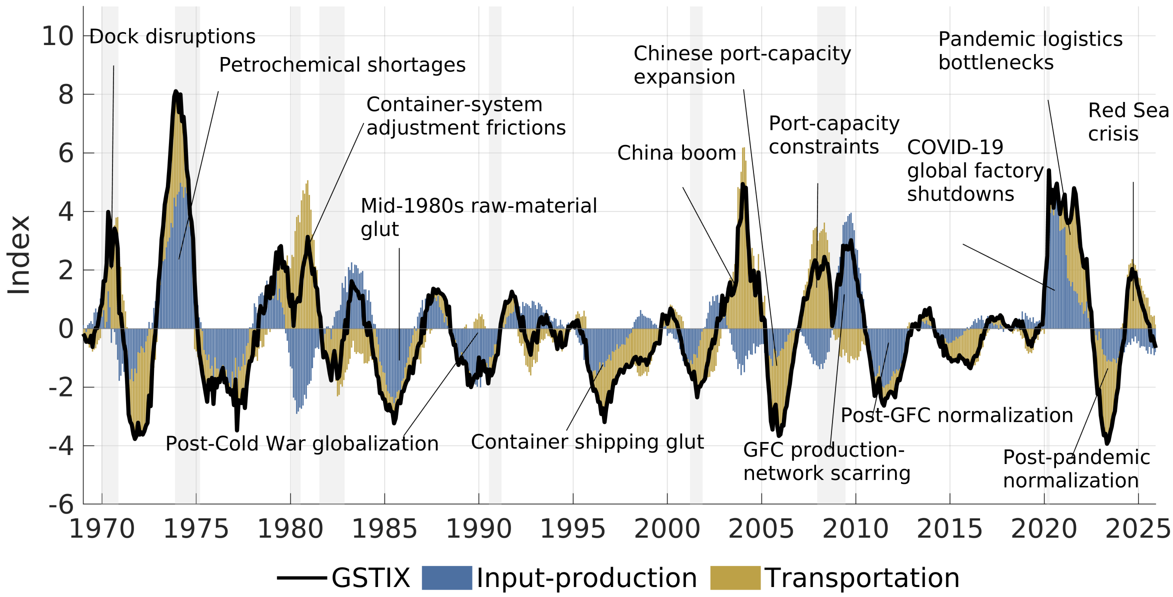

Notes: Vertical grey bars denote NBER U.S. recessions. Positive values indicate above-average global supply-chain tensions, while negative values indicate below-average tensions. Panel (a) reports the composite Global Supply Chain Tension Index (GSTIX), obtained by summing the historical contributions of transportation and input-production supply shocks to supplier delivery times and real transportation costs. The solid black line denotes the posterior mean, while the dark and light shaded areas indicate the 68% and 90% robust credible regions, respectively. Panel (b) decomposes the posterior-mean GSTIX into the contributions of transportation and input-production tensions. Labels highlight selected historical episodes that illustrate the dominant source of supply-chain tensions.

changed (Section 3.4.1), suggesting that GSTIX captures these broader supply-chain dimensions of energy crises rather than merely reflecting oil-price fluctuations.

Panel (b) decomposes these aggregate movements into transportation and input-production tensions.[3] The decomposition illustrates a main finding of the paper: episodes with similar levels of aggregate supply-chain tension can have very different structural origins. The pandemic provides a particularly clear example. At its onset, factory closures and interruptions to the availability of intermediate inputs generate a predominantly input-production episode. As production and trade recovered, the composition gradually shifted toward transportation disturbances, reflecting port bottlenecks, container imbalances, limited shipping capacity, and the difficulties of repositioning logistics networks. This temporal sequence is consistent with evidence that the initial containment measures produced sharp production and trade losses, while congestion and shipping delays accelerated later in the pandemic.

The 2003–04 global trade boom provides a particularly informative example of diverging supply-chain conditions. Transportation tensions rise markedly as the rapid expansion of global trade, associated in part with China's integration into the world economy, presses against available shipping capacity. At the same time, input-production tensions ease amid the expansion of global manufacturing capacity and China's increasing integration into global production networks. The opposing movements illustrate how aggregate supply-chain stress can mask markedly different conditions in transportation and input production.

To complete the decomposition of global supply-chain tensions, we use the third structural shock to construct the *Global Supply Chain Congestion Index* (GSCIX):

$$\mathrm{GSCIX}_t = \widetilde{HD}_{s,t}^{\mathrm{CONG}} + \widetilde{HD}_{z,t}^{\mathrm{CONG}}.$$

Since the GSCIX is built from the historical decomposition of transportation cost and supplier delivery time due to the congestion shock, it captures movements in these two series that are predominantly associated with demand-induced expansions in global manufacturing, while allowing other forces associated with stronger utilization of global production and logistics networks to contribute. Fig. 5 shows that congestion increases during periods of strong global expansion and post-recession recoveries, while declining sharply during global downturns. The pandemic again illustrates the distinction between congestion and supply-side tensions. The initial lockdowns and factory shutdowns appear as a relaxation of congestion, reflecting the collapse in global activity. As economies reopened, however, expenditure rotated from services toward goods and merchandise trade rebounded rapidly, placing increasing pressure on transportation networks. Smith et al. (2023) document that retail inventories were depleted early in the pandemic, followed by a surge in imports roughly four months later that

[3] Appendix C.2 reports the two source-specific indices separately, together with their robust credible regions, and compares the composite GSTIX with existing measures of supply-chain stress.

contributed to persistent port congestion. This narrative evolution closely mirrors the decomposition in Fig. 4: input-production disruptions dominate the initial phase of the pandemic in early 2020, whereas transportation tensions become increasingly important from late 2020 throughout 2021.

Figure 5: Historical episodes of congestion in global supply chains

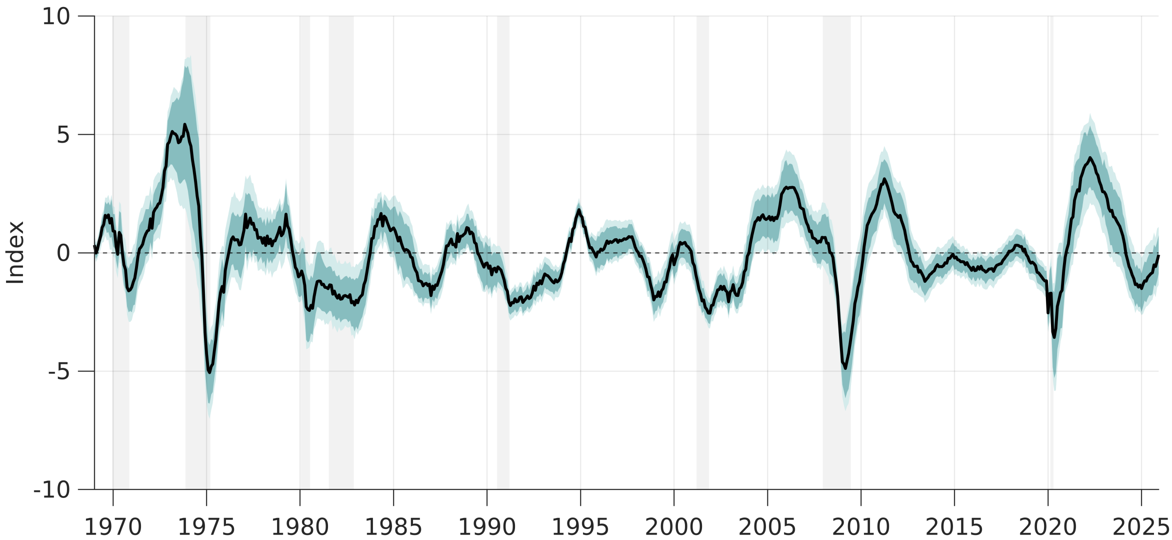

Notes: The Global Supply Chain Congestion Index (GSCIX) is constructed from the standardized historical contributions of the congestion shock to the supplier-delivery-times index and real transportation costs. While congestion is primarily associated with demand-driven expansions, its interpretation extends to other factors, such as technological shifts that raise production without proportionate increases in transportation capacity or input availability. The solid black line is the mean under the reference distribution over admissible rotations; dark and light shaded areas denote the 68% and 90% robust credible regions.

Having separated supply-side tensions from congestion, we next compare the resulting measures with existing indicators of supply-chain stress. The historical signal in GSTIX is broadly consistent with existing indicators, while differing in informative ways. Appendix Figure C.3 compares GSTIX with the Global Supply Chain Pressure Index (GSCPI) of Benigno et al. (2022), the newspaper-based U.S. Supply Bottlenecks Index of Burriel et al. (2024), and the U.S. Shortage Index of Caldara et al. (2025). All four identify the pandemic as an exceptional period of supply-chain stress, but they differ noticeably in volatility and persistence. The newspaper-based Shortage Index displays the sharpest event-specific spikes, followed by the Supply Bottlenecks Index, while the GSCPI and especially GSTIX evolve more smoothly. For GSTIX, this smoothness partly reflects its dynamic construction: the index incorporates the continuing historical contributions of past structural shocks rather than measuring only contemporaneous conditions. The same feature generates an economically distinct signal during normalization. As adverse disruptions unwind, their historical contributions can turn negative, so GSTIX can indicate an easing of supply-side tensions rather than simply returning toward its historical mean.

The correlations reported in Appendix Table C.1 further illustrate the importance of distinguishing the sources of supply-chain tensions. Over the common sample 1998–2025, the composite supply-side GSTIX is positively correlated with all three alternative indicators, with correlations ranging from 0.20 for the U.S. Shortage Index to 0.50 for the GSCPI. These correlations increase markedly when the congestion component is added to GSTIX, reaching 0.49, 0.51, and 0.72 for the Shortage Index, SBI, and GSCPI, respectively. The same pattern prevails over the longer overlapping samples available for the SBI and Shortage Index, with correlations increasing from 0.33 to 0.50 and from 0.44 to 0.58, respectively. This systematic increase is consistent with existing indicators capturing broader manifestations of supply-chain pressure without distinguishing adverse supply disruptions from congestion associated primarily with strong global activity. GSTIX deliberately isolates transportation and input-production supply disruptions, whereas adding GSCIX restores the third source of supply-chain tensions identified by our model.

3.4 Robustness

This section examines three broad robustness concerns: changes in the information set of the structural VAR, sensitivity to the COVID-19 episode, and sensitivity to the selection of narrative events.

3.4.1 Robustness to the inclusion of oil prices

Because energy-market disturbances can affect production costs, transportation demand, and the availability of intermediate inputs, we assess whether adding the real price of oil to the global information set materially changes the identified transportation and input-production responses. This exercise should be interpreted as a sensitivity check to oil-price information; it does not by itself establish that the baseline input-production shock is orthogonal to a separately identified oil-supply shock.

Fig. 6 shows that the impulse responses remain remarkably similar to the baseline specification. Including oil prices leads to somewhat wider robust credible regions and slightly smaller long-run effects on industrial production, suggesting that part of the persistence associated with supply-chain disruptions is transmitted through energy markets. Nevertheless, the qualitative responses remain largely unchanged, indicating that the identified transportation and input-production shocks capture broader supply-chain mechanisms rather than merely proxying for oil-price fluctuations.

Figure 6: Robustness to inclusion of the oil price

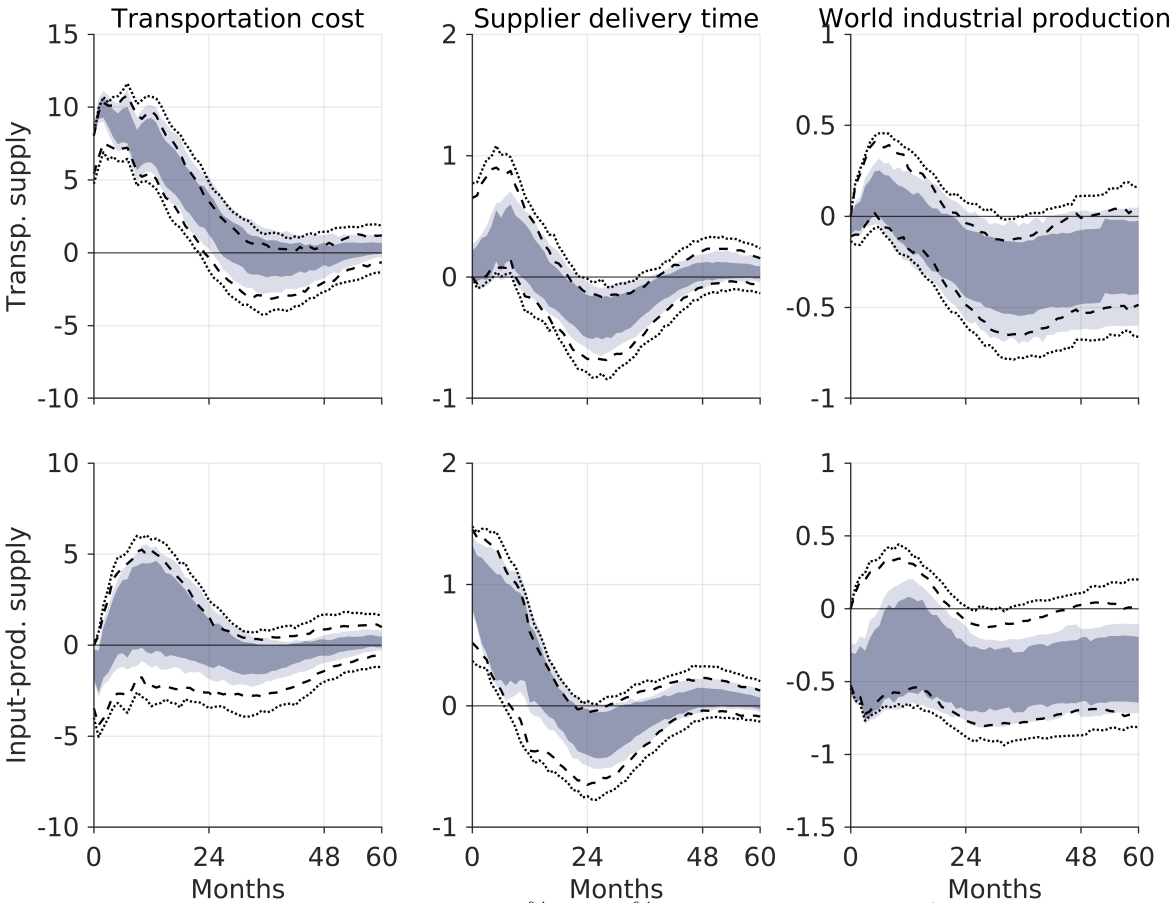

Notes: Dashed and dotted lines denote the 68% and 90% robust credible regions for impulse responses from the robustness specification that augments the baseline SVAR with the real price of oil while maintaining the same identifying restrictions. Shaded areas report the 68% and 90% robust credible regions of the baseline specification. Responses are shown for the three baseline variables only.

3.4.2 Robustness to the COVID-19 episode

A natural concern is that the estimated transmission mechanisms may be driven disproportionately by the COVID-19 pandemic, the largest supply-chain disruption in recent history. If the identified impulse responses primarily reflected this exceptional episode, their relevance for earlier supply-chain disruptions would be limited. To address this concern, we re-estimate the model using data only through December 2019, thereby excluding the pandemic and its aftermath while maintaining the same identifying restrictions.

Fig. 7 shows that the impulse responses remain remarkably similar to the baseline specification. Excluding the COVID-19 period leaves the broad sign and persistence patterns qualitatively similar, although the robust regions widen for several responses. We therefore view the pre-COVID specification as evidence that the baseline results are not mechanically generated by the largest pandemic observations, while recognizing

Figure 7: Robustness to the COVID-19 episode

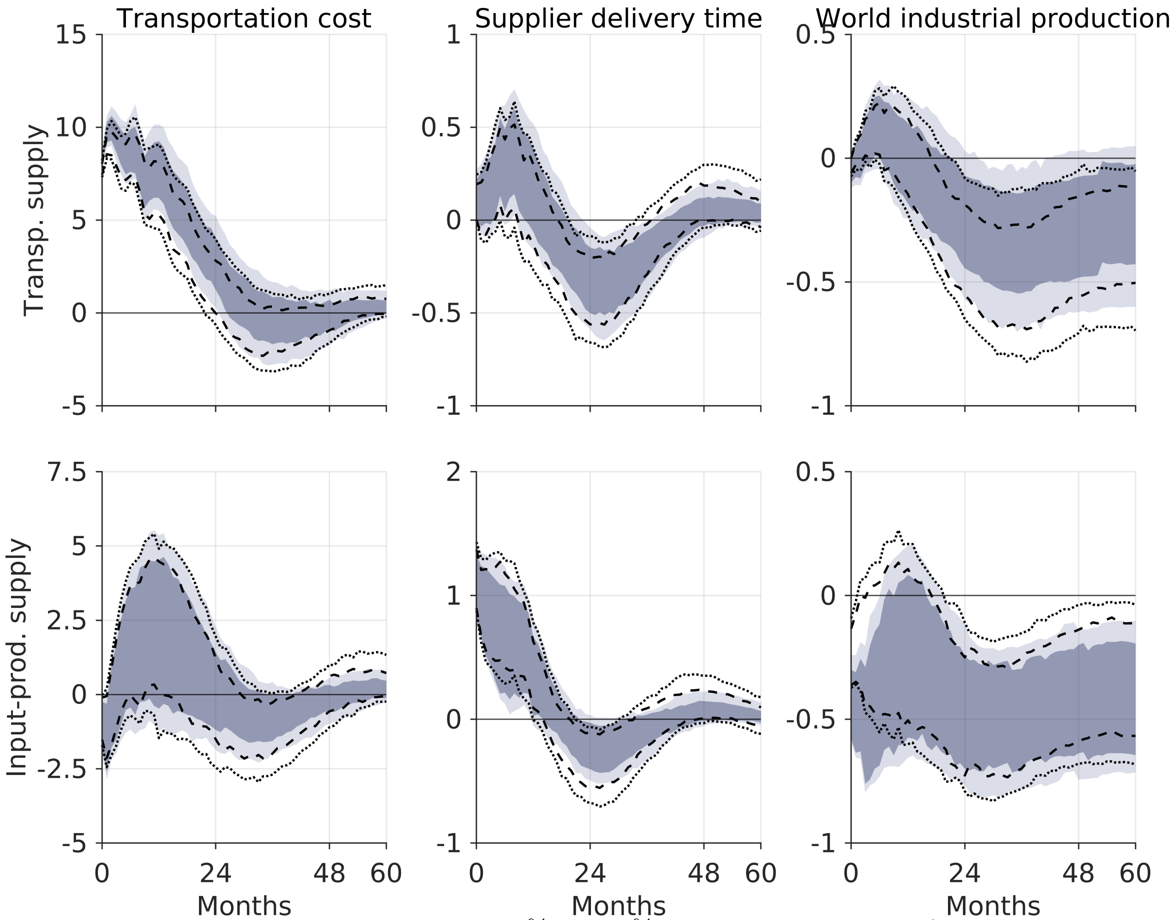

Notes: Dashed and dotted lines denote the 68% and 90% robust credible regions for impulse responses from the robustness specification estimated over the pre-COVID sample (1968m1–2019m12). Shaded areas report the 68% and 90% robust credible regions of the baseline specification.

that the shorter sample provides less information about some responses.

3.4.3 Robustness to narrative-event selection

Narrative restrictions require judgement in selecting and classifying historical episodes. To assess whether the baseline results depend critically on any single episode, we conduct a leave-one-event-out exercise, re-estimating the model thirteen times while excluding one narrative event in each specification. Figure 8 reports the envelope of the resulting robust regions. This exercise addresses influence of individual events.

The resulting impulse responses remain remarkably similar to the baseline specification. Excluding individual narrative events leads to a moderate widening of the uncertainty bands, particularly for the long-run responses following input-production shocks, while leaving the qualitative responses and their persistence largely unchanged. Overall, the results indicate that the narrative restrictions contribute jointly to identification and that the estimated transmission mechanisms do not depend critically on

Figure 8: Robustness to narrative-event selection

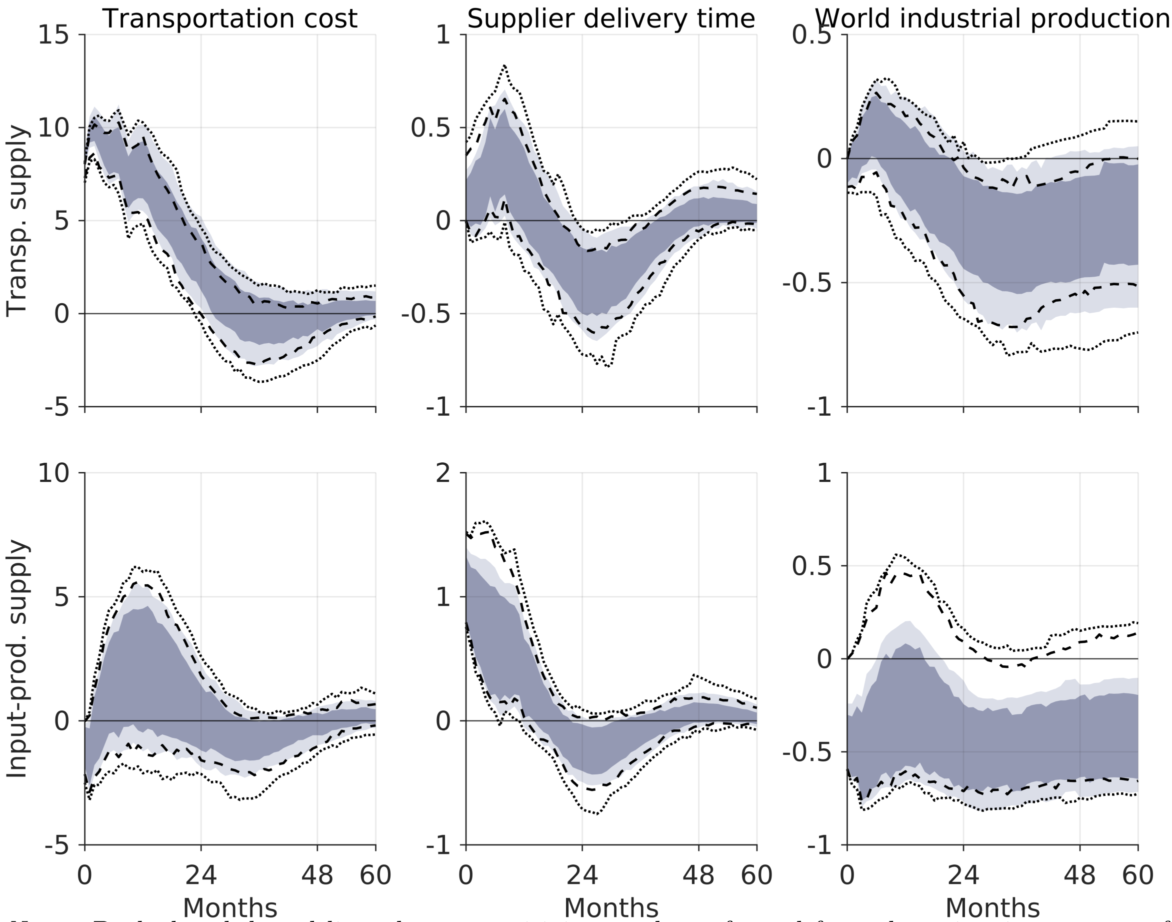

Notes: Dashed and dotted lines denote sensitivity envelopes formed from the pointwise extrema of the 68% and 90% robust credible regions across the thirteen leave-one-event-out specifications. These envelopes summarize cross-specification sensitivity and should not be interpreted as posterior credible regions from a single model. Shaded areas report the baseline robust credible regions.

any single historical episode.

4 Macroeconomic effects

4.1 Block-exogenous VAR

We trace the macroeconomic effects of the identified global shocks using a monthly block-exogenous VAR following Cushman and Zha (1997). The specification treats the three-variable global block as predetermined with respect to the U.S. block: identified global shocks can affect U.S. variables contemporaneously and with lags, whereas U.S.-block variables do not feed back into the global equations. This is a maintained modeling restriction rather than a literal small-open-economy assumption, since some global indicators contain U.S. information. We therefore interpret the exercise as a conditional propagation analysis of the externally identified global disturbances.

Let $\boldsymbol{Y}_t$ collect the three baseline global variables—transportation cost s_t, supplier delivery time z_t, and world industrial production g_t—ordered as $(s_t, z_t, g_t)'$. The global block is estimated and structurally identified as described in Section 2. Conditional on each admissible structural parameterization, the U.S. block is estimated by OLS according to

$$\begin{bmatrix} \boldsymbol{Y}_t \\ \boldsymbol{X}_t \end{bmatrix} = \begin{bmatrix} \boldsymbol{a}_c \\ \boldsymbol{c}_c \end{bmatrix} + \begin{bmatrix} \boldsymbol{a}_t \\ \boldsymbol{c}_t \end{bmatrix} + \begin{bmatrix} \boldsymbol{A}(L) & \boldsymbol{0} \\ \boldsymbol{C}(L) & \boldsymbol{D}(L) \end{bmatrix} \begin{bmatrix} \boldsymbol{Y}_t \\ \boldsymbol{X}_t \end{bmatrix} + \begin{bmatrix} \boldsymbol{B} & \boldsymbol{0} \\ \boldsymbol{E} & \boldsymbol{F} \end{bmatrix} \begin{bmatrix} \boldsymbol{\varepsilon}_t^Y \\ \boldsymbol{\varepsilon}_t \end{bmatrix}, \tag{9}$$

with $p = 12$ lags and a deterministic trend. The vectors $\boldsymbol{a}_c$ and $\boldsymbol{c}_c$ contain the intercepts of the global and U.S. blocks, respectively, while $\boldsymbol{a}_t$ and $\boldsymbol{c}_t$ denote the corresponding coefficients on a linear time trend. The identified global supply-chain shocks ε_t^Y enter the U.S. block contemporaneously through $\boldsymbol{E}$, while the upper-right zero blocks exclude contemporaneous and lagged feedback from the U.S. block to the global block.[4] We do not identify shocks originating within the U.S. block. Accordingly, $\boldsymbol{F}\boldsymbol{\varepsilon}_t$ represents the unrestricted U.S.-block innovations.

The matrix containing the U.S. data series $\boldsymbol{X}_t$ comprises industrial production, business inventories, headline and core PCE prices, services prices, the producer price index, the one-year Treasury rate, and the unemployment rate. The model is estimated from January 1968 to December 2025; Appendix B.1 describes the data. Uncertainty about the identification of the global shocks is propagated into the U.S. responses. For each admissible global structural parameterization, we recover the global shocks, estimate the U.S. block by OLS conditional on those shocks, and compute impulse

[4] Block exogeneity allows us to focus on the transmission of the externally identified global supply-chain shocks to the U.S. economy. Allowing U.S. developments to feed back into global conditions would require modeling the joint determination of global and U.S. disturbances, which is beyond the scope of our analysis.

responses from the implied block-exogenous VAR. The reported 68% and 90% regions therefore reflect uncertainty from the global reduced form and structural identification conditional on plug-in estimates of the U.S.-block coefficients. They do not incorporate additional sampling uncertainty from those domestic coefficients.

4.2 Dynamic response of the U.S. economy

We next quantify how the identified global transportation and input-production shocks propagate to the U.S. economy. Fig. 9 reports impulse responses for output, inventories, price levels, labor-market conditions, and the one-year Treasury yield. The bands reflect uncertainty in the identified global shocks conditional on the estimated U.S.-block coefficients.

A transportation shock generates a temporary stagflationary pattern in the U.S. block. Industrial production declines and inventories are gradually depleted as the disruption propagates. Producer and consumer price levels increase, with the producer-price response peaking earlier and the consumer-price responses flattening over medium horizons.[5] The unemployment rate rises gradually, while the one-year Treasury yield shows little evidence of a sustained increase. Overall, the responses are consistent with a comparatively transitory cost-push episode.

Input-production shocks generate a more persistent stagflationary pattern. Industrial production and inventories remain below baseline over the reported horizon, while unemployment rises persistently. The producer and consumer price levels also display more persistent increases than after transportation shocks. The one-year Treasury yield rises persistently, a pattern consistent with higher expected short-term rates and/or changes in term premia in response to the more durable macroeconomic effects of the disturbance. The comparison reveals a clear difference in propagation across the two adverse supply disturbances. Transportation shocks are associated with comparatively transitory price-level responses, whereas input-production shocks generate more persistent responses of inventories, activity, labor-market conditions, and consumer price levels. The one-year Treasury yield also responds more persistently to input-production shocks. These differences provide a structural interpretation for why supply-chain disruptions with similar observable symptoms may have different macroeconomic persistence.

On the real activity side, foundational work by Acemoglu et al. (2012) shows that input-output linkages transmit sectoral shocks to the aggregate economy and generate cascade effects when some sectors occupy central positions in production networks.

[5] See also Carrière-Swallow et al. (2023) and Känzig and Raghavan (2025) on the pass-through of shipping-cost shocks to producer and consumer prices.

Figure 9: Transmission of global supply-chain shocks to the U.S. economy

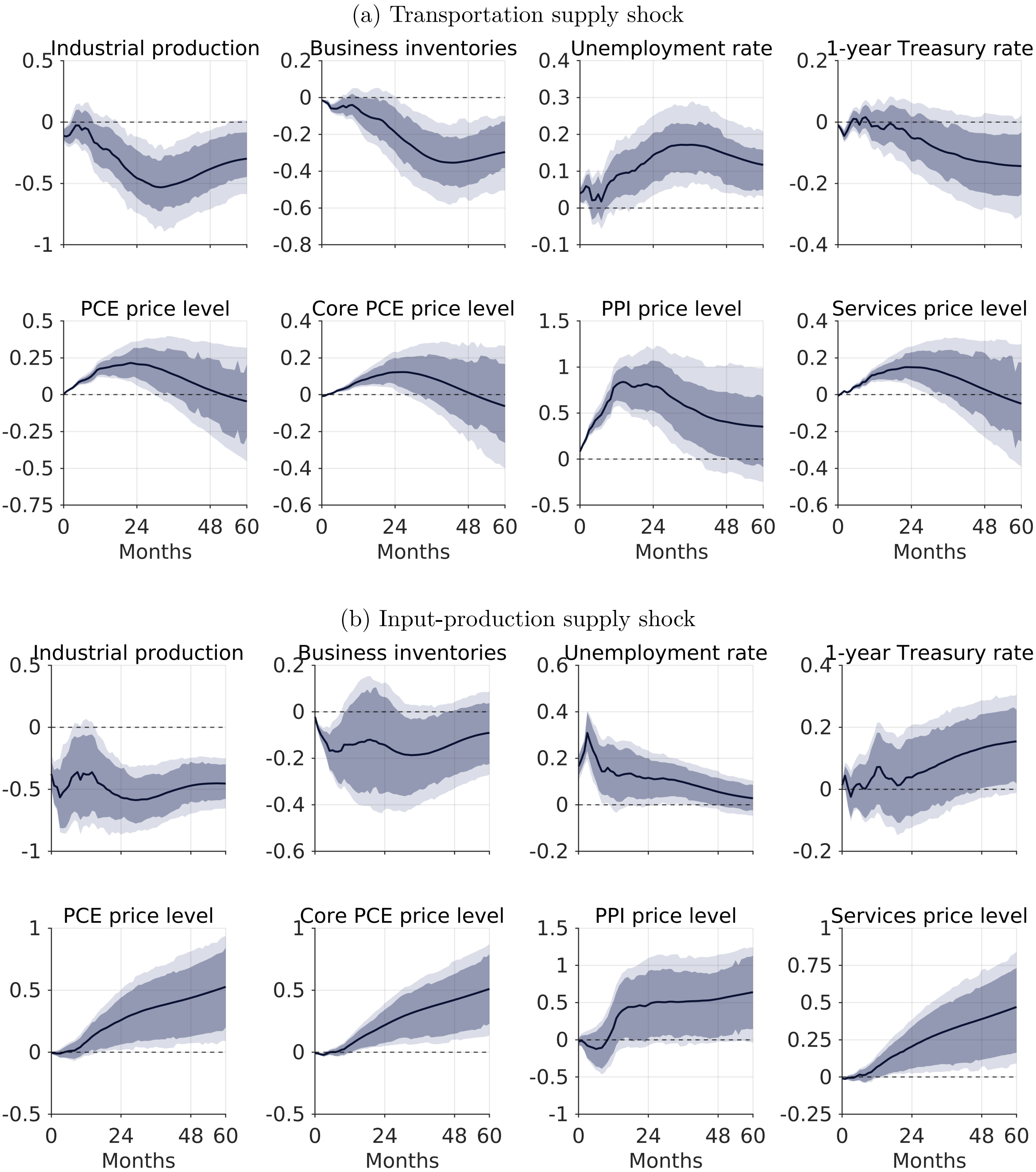

Notes: Impulse responses of U.S. macroeconomic variables to one-standard-deviation global transportation and input-production shocks. Global shocks are identified in the baseline SVAR and enter the U.S. block contemporaneously through the block-exogenous VAR. Dark and light shaded bands denote the 68% and 90% regions reflecting global identification uncertainty conditional on the estimated U.S.-block coefficients. Responses of industrial production, business inventories, and the PCE, core PCE, services, and producer price levels are cumulative percentage deviations from the pre-shock path. The unemployment rate and the one-year Treasury yield are measured in percentage points.

Such propagation can be amplified by market structure, entry, and exit (Baqaee, 2018). An additional source of persistence arises from firm-to-firm relationships: established international trading relationships are valuable and costly to replace (Monarch and Schmidt-Eisenlohr, 2023), while Acemoglu and Tahbaz-Salehi (2025) show theoretically that supply disruptions can induce the breakdown of relationship-specific supplier–customer links and thereby trigger further contractions in production networks and aggregate output. Together, these mechanisms limit the economy's ability to substitute away from disrupted inputs and suppliers and can amplify the initial disruption, providing a rationale for the persistent output effects we find in response to input-production shocks.

On the inflation side, Nakov and Ghassibe (2025) provide a particularly relevant theoretical mechanism, showing that upstream supply shocks generate persistent inflation through pricing cascades in production networks. Consistent with this mechanism, recent firm-level evidence documents persistent producer-price adjustments following supply-chain disruptions (Finck et al., 2026), while aggregate evidence points to persistent inflationary effects of supply-chain pressures (Ascari et al., 2024). Our results add that persistence differs across the structural components identified in our model: the input-production component is associated with more persistent U.S. price-level responses than the transportation component.

4.3 U.S. pandemic-era inflation

We next use the historical decomposition of the block-exogenous VAR to assess the contribution of global supply-chain disturbances to U.S. PCE inflation during and after the pandemic. Fig. 10 reports the quarterly decomposition, while Tab. 4 summarizes annual contributions over 2020–2025. Point contributions shown in the figure and table are means under the reference distribution used to summarize admissible structural parameterizations; the accompanying robust regions characterize identification uncertainty. The chronology reveals substantial variation in both the size and composition of supply-chain pressures. In 2020, the inflationary contributions of the two adverse supply shocks were more than offset by a large negative demand-induced congestion contribution. In 2021, transportation and input-production shocks jointly contributed about 3.3 percentage points to PCE inflation, with nearly identical reference-distribution mean contributions from the two sources.

Supply-chain pressures remained important in 2022, but their composition shifted. Transportation and input-production shocks jointly contributed about 2.4 percentage points to PCE inflation, with the input-production component accounting for roughly 1.8 percentage points and transportation for about 0.6 percentage point under the reference distribution. At the same time, the activity-induced congestion component became inflationary as strong activity pressed against constrained production and logistics capacity (Ferrante et al., 2023; Fornaro and Romei, 2022). The decomposition therefore suggests that the persistence of supply-chain-related price pressures cannot be attributed solely to the initial transportation bottlenecks: the input-production component remained inflationary after the most acute logistics disruptions had begun to ease.

Table 4: U.S. PCE inflation, annual historical-decomposition contributions

Shock	Statistic	2020	2021	2022	2023	2024	2025
Transportation	Mean	0.72	1.66	0.61	-0.90	0.20	0.36
	68% interval	[-0.04, 1.11]	[1.00, 2.25]	[-0.09, 1.32]	[-1.40, -0.08]	[-0.39, 0.84]	[-0.15, 1.05]
	90% interval	[-0.40, 1.68]	[0.54, 2.71]	[-0.67, 1.77]	[-2.02, 0.33]	[-0.97, 1.28]	[-0.81, 1.53]
Input production	Mean	0.36	1.65	1.82	1.38	1.09	0.88
	68% interval	[-1.04, 1.58]	[-0.15, 2.87]	[0.08, 3.30]	[-0.24, 2.79]	[-0.65, 2.29]	[-0.58, 2.10]
	90% interval	[-1.48, 2.62]	[-0.42, 4.17]	[-0.62, 4.40]	[-0.65, 4.09]	[-0.88, 3.71]	[-1.22, 3.35]
Congestion	Mean	-1.62	-0.09	1.48	1.92	0.79	0.35
	68% interval	[-3.12, -0.19]	[-1.54, 1.84]	[-0.38, 3.36]	[0.28, 3.78]	[-0.94, 2.43]	[-1.45, 1.74]
	90% interval	[-3.69, 1.05]	[-2.36, 2.70]	[-1.17, 4.11]	[-0.31, 4.79]	[-1.52, 3.60]	[-2.05, 3.06]

Notes: Entries report annual historical-decomposition contributions of global transportation, input-production, and global activity-induced congestion shocks to U.S. PCE inflation, in percentage points. For each shock and year, the first row reports the reference-distribution mean. The following rows report 68% and 90% regions reflecting uncertainty from the identified global shocks conditional on the estimated U.S.-block coefficients. Marginal interval endpoints should not be added across shocks.

The subsequent disinflation also differed by source. In 2023, the normalization of transportation conditions subtracted approximately 0.9 percentage point from PCE inflation, whereas input-production shocks continued to contribute about 1.4 percentage points. The net contribution of the two adverse supply shocks was therefore modestly

Figure 10: Contributions to U.S. PCE inflation (2019:IV-2025:IV)

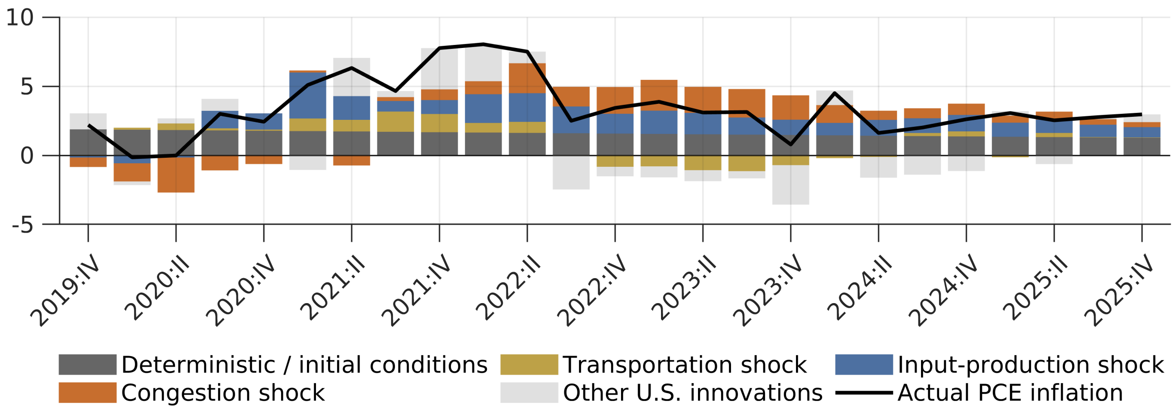

Notes: Historical decomposition of quarterly U.S. PCE inflation from the block-exogenous VAR. Stacked bars report reference-distribution mean contributions of transportation, input-production, and global-demand-induced congestion shocks, U.S.-block innovations, and deterministic terms and initial conditions. The solid black line denotes observed annualized quarter-on-quarter PCE inflation. Contributions are measured in percentage points and add to observed inflation up to numerical approximation. The stacked-bar means are descriptive summaries under the reference distribution and are not themselves prior-robust objects.

positive, at around 0.5 percentage point, while congestion remained highly inflationary. Transportation normalization thus contributed materially to disinflation, but its effect was partly offset by the more persistent transmission of input-production disruptions and continued pressure on available capacity. By 2024 and 2025, the posterior-mean contributions of the adverse supply shocks remained positive, although the associated robust credible regions were wide and generally included zero. This evolution mirrors the impulse responses, according to which transportation disturbances generate comparatively transitory inflationary effects, whereas input-production disruptions propagate much more persistently through production networks.

These findings complement a growing literature attributing an important role to global supply-chain disturbances during the post-pandemic inflation episode. Bernanke and Blanchard (2025), for example, conclude that shocks originating in commodity and product markets accounted for much of the initial inflation surge before labor-market tightness became more important for inflation persistence. Our results are consistent with this evidence, but provide a more granular structural assessment. In particular, we show that transportation disruptions contributed primarily to the inflation take-off before becoming disinflationary as logistics conditions normalized, whereas input-production disruptions generated smaller initially but considerably more persistent inflationary pressures.

Overall, the results suggest that global supply-chain disturbances accounted for a sizable, but incomplete, share of pandemic-era U.S. inflation. Domestic innovations, activity-induced congestion, and other macroeconomic forces remain quantitatively important, consistent with studies emphasizing aggregate demand, monetary policy, and labor-market tightness (Giannone and Primiceri, 2024; Bocola et al., 2024; Benigno and Eggertsson, 2023). The decomposition therefore reconciles these perspectives: global supply-chain disturbances materially amplified inflation, but neither adverse supply shocks nor activity-induced congestion alone can account for the full episode. Our estimates complement the larger supply-side contributions found by Ferrante et al. (2023) and di Giovanni et al. (2022). The difference is informative about measurement: our structural decomposition separately attributes observed inflation dynamics to distinct adverse supply-chain disturbances, activity-induced congestion, and domestic innovations.

5 Conclusion

We develop a parsimonious structural VAR that identifies three distinct sources of global supply-chain tensions: transportation supply shocks, input-production supply shocks, and congestion associated primarily with expansions in global activity. Our central finding is that observationally similar supply-chain tensions can originate from economically distinct disturbances with markedly different macroeconomic propagation. Consequently, neither supplier delivery times nor transportation costs constitute a sufficient statistic for supply-chain stress, since both reflect the combined effects of transportation disruptions, input-production shortages, and congestion.

The historical decomposition yields monthly source-specific indicators for 1969–2025. The GSTIX components distinguish transportation from input-production tensions and capture the dynamic contribution of both current and past disturbances. They should therefore be interpreted as model-based decompositions of observed supply-chain stress rather than as direct physical measures of disruptions.

In the U.S. economy, both adverse supply disturbances are contractionary and inflationary, but their propagation differs markedly. Transportation disruptions are associated with comparatively transitory price-level responses, whereas input-production disruptions generate more persistent responses of inventories, industrial production, employment, and consumer price levels. The one-year Treasury yield also rises more persistently after input-production shocks. During the post-pandemic episode, transportation and input-production contributions evolved differently, with transportation becoming disinflationary as logistics conditions normalized while the input-production component remained inflationary for longer.

These differences have direct implications for monetary-policy assessment. Similar increases in commonly monitored indicators such as supplier delivery times can be associated with different degrees of inflation persistence depending on whether they originate in transportation disruptions, input-production shortages, or congestion. The intensity of observed supply-chain stress is therefore not sufficient for evaluating its macroeconomic consequences: identifying its source provides information about the likely persistence of inflation and the associated policy trade-offs. In particular, the normalization of transportation conditions need not imply that supply-side inflationary pressures have dissipated when input-production disruptions continue to propagate through production networks. Source-specific measures such as GSTIX can therefore complement aggregate supply-chain indicators in the real-time assessment of inflationary pressures.

References

Acemoglu, D., Carvalho, V., Ozdaglar, A., and Tahbaz-Salehi, A. (2012). The network origins of aggregate fluctuations. *Econometrica*, 80(5):1977–2016.

Acemoglu, D. and Tahbaz-Salehi, A. (2025). The macroeconomics of supply chain disruptions. *Review of Economic Studies*, 92(2):656–695.

Afrouzi, H. and Bhattarai, S. (2023). Inflation and GDP dynamics in production networks: A sufficient statistics approach. NBER Working Paper No. 31218.

Alessandria, G., Khan, S. Y., Khederlarian, A., Mix, C., and Rhul, K. J. (2023). The aggregate effects of global and local supply chain disruptions: 2020-2022. *Journal of International Economics*, 146:103788.

Antolin-Diaz, J. and Rubio-Ramirez, J. F. (2018). Narrative sign restrictions for SVARs. *American Economic Review*, 108(10):2802–2829.

Ascari, G., Bonam, D., and Smădu, A. (2024). Global supply chain pressure shocks and inflation in the euro area. *Journal of International Money and Finance*, 142:103022.

Bai, X., Fernandez-Villaverde, J., Li, Y., and Zanetti, F. (2026). The causal effects of global supply chain disruptions on macroeconomic outcomes: Evidence and theory. *American Economic Review*. Forthcoming.

Baqaee, D. R. (2018). Cascading failures in production networks. *Econometrica*, 86(5):1819–1838.

Barrot, J.-N. and Sauvagnat, J. (2016). Input specificity and the progagation of idiosyncratic shocks in production networks. *Quarterly Journal of Economics*, 131(3):1543–1592.

Baumeister, C. and Hamilton, J. (2019). Structural interpretation of vector autoregressions with incomplete identification: Revisiting the role of oil supply and demand shocks. *American Economic Review*, 109(5):1873–1910.

Baumeister, C. and Hamilton, J. D. (2015). Sign restrictions, structural vector autoregressions, and useful prior information. *Econometrica*, 83(5):1963–1999.

Benigno, G., di Giovanni, J., Groen, J. J., and Noble, A. I. (2022). The GSCPI: A new barometer of global supply chain pressures. Federal Reserve Bank of New York Staff Papers No. 1017.

Benigno, P. and Eggertsson, G. B. (2023). It's baaack: The surge in inflation in the 2020s and the return of the non-linear Phillips curve. NBER Working Paper No. 31197.

Bernanke, B. S. and Blanchard, O. J. (2025). What caused the US pandemic-era inflation? *American Economic Journal: Macroeconomics*, 17(3):1–35.

Bocola, L., Dovis, A., Jørgensen, K., and Kirpalani, R. (2024). Bond market views of the Fed. NBER Working Paper No. 32620.

Boehm, C. E., Flaaen, A., and Pandalai-Nayar, N. (2019). Input linkages and the transmission of shocks: Firm-level evidence from the 2011 Tōhoku earthquake. *Review of Economics and Statistics*, 101(1):60–75.

Brancaccio, G., Kalouptsidi, M., and Papageorgiou, T. (2025a). Rigidities in transportation and supply chain disruptions. NBER Working Paper No. 33452.

Brancaccio, G., Kalouptsidi, M., and Papageorgiou, T. (2025b). Rigidities in transportation and supply chain disruptions. *AEA Papers and Proceedings*, 115:543–550.

Burriel, P., Kataryniuk, I., Monero Pérez, C., and Viani, F. (2024). A new supply bottleneck index based on newspaper data. *International Journal of Central Banking*, 20(2):17–67.

Caldara, D., Iacoviello, M., and Yu, D. (2025). Measuring shortages since 1900. Board of Governors of the Federal Reserve System International Finance Discussion Paper No. 1407.

Carrière-Swallow, Y., Deb, P., Furceri, D., Jiménez, D., and Ostry, J. D. (2023). Shipping costs and inflation. *Journal of International Money and Finance*, 130:102771.

Carvalho, V., Nirei, M., Saito, Y., and Tahbaz-Salehi, A. (2021). Supply chain disruptions: Evidence from the Great East Japan earthquake. *Quarterly Journal of Economics*, 136(2):1255–1321.

Comin, D. A., Johnson, R. C., and Jones, C. J. (2023). Supply chain constraints and inflation. NBER Working Paper No. 31179.

Cushman, D. O. and Zha, T. (1997). Identifying monetary policy in a small open economy under flexible exchange rates. *Journal of Monetary Economics*, 39(3):433–448.

Dhyne, E., Kikkawa, A., Mogstad, M., and Tintelnot, F. (2021). Trade and domestic production networks. *Review of Economic Studies*, 88(2):643–668.

di Giovanni, J., Kalemli-Özcan, S., Silva, A., and Yildirim, M. A. (2022). Global supply chain pressures, international trade, and inflation. NBER Working Paper No. 30240.

Ferrante, F., Graves, S., and Iacoviello, M. (2023). The inflationary effects of sectoral reallocation. *Journal of Monetary Economics*, 140(Supplement):S64–S81.

Finck, D., Klein, M., and Tillmann, P. (2026). Global supply chain disruptions and producer price inflation: Evidence from swedish firms. *European Economic Review*, 189:105426.

Fornaro, L. and Romei, F. (2022). Monetary policy during unbalanced global recoveries. CEPR Discussion Paper No. 16971.

Fuchs, S. and Wong, W. F. (2026). Multimodal transport networks. NBER Working Paper No. 35065.

Giacomini, R. and Kitagawa, T. (2021). Robust Bayesian inference for set-identifed models. *Econometrica*, 89(4):1519–1556.

Giacomini, R., Kitagawa, T., and Read, M. (2023). Identification and inference under narrative restrictions. Reserve Bank of Australia Research Discussion Paper No. RDP 2023-07.

Giannone, D. and Primiceri, G. E. (2024). The drivers of post-pandemic inflation. NBER Working Paper No. 32859.

Hamilton, J. D. (2019). Measuring global economic activity. *Journal of Applied Econometrics*, 36(3):293–303.

Hummels, D. and Schaur, G. (2013). Time as a trade barrier. *American Economic Review*, 103(7):2935–2959.

Känzig, D. R. and Raghavan, R. (2025). The macroeconomic effects of supply chain shocks: Evidence from global shipping disruptions. Northwestern University Working Paper.

Kilian, L. (2009). Not all oil price shocks are alike: Disentangling demand and supply shocks in the crude oil market. *American Economic Review*, 99(3):1053–1069.

Kilian, L. and Murphy, D. P. (2012). Why agnostic sign restrictions are not enough: Understanding the dynamics of oil market VAR models. *Journal of the European Economic Association*, 10(5):1166–1188.

Lee, K. and Ni, S. (2002). On the dynamic effects of oil price shocks: A study using industry level data. *Journal of Monetary Economics*, 49(4):823–852.

Monarch, R. and Schmidt-Eisenlohr, T. (2023). Longevity and the value of trade relationships. *Journal of International Economics*, 145:103842.

Nakov, A. and Ghassibe, M. (2025). Business cycles with pricing cascades. European Central Bank Working Paper No. 3123.

Rubbo, E. (2023). Networks, Phillips curves, and monetary policy. *Econometrica*, 91(4):1417–1455.

Rubio-Ramírez, J. F., Waggoner, D. F., and Zha, T. (2010). Structural vector autoregressions: Theory of identification an algorithm for inference. *Review of Economic Studies*, 77:665–696.

Smith, D., Bingham, P., Hackett, D., and Smith, J. (2023). Multiperspective analysis of pandemic impacts on U.S. import trade: What happened, and why. *Transportation Research Record*, 2678(1):45–61.

Online Appendix

The Sources of Global Supply Chain Tensions

by M. Elsayed*, C. Grosse-Steffen‡ and M. Marx§

Banque de France, 31 rue des Petits-Champs, 75001 Paris, France.

This Online Appendix contains four parts. Appendix A develops the theoretical production-network model that underpins the identification strategy for sign-restrictions. Appendix B describes all data sources and details the construction of the transportation-cost index. Appendix C collects complementary empirical results. Appendix D provides a detailed description of the narrative episodes and their economic impact.

A Theoretical model

This appendix develops a simple production-network framework that rationalizes the sign restrictions used to identify the empirical SVAR, in particular the differential response of transportation costs to transportation and input-production disruptions. The model is not intended to provide a quantitative assessment. It is deliberately static because its sole purpose is to motivate contemporaneous identifying restrictions; dynamic propagation is estimated nonparametrically in the SVAR. The model also does not feature occasionally binding capacity constraints, which are instead subsumed in the empirical congestion shock identified after the two supply-side shocks have been characterized.

A.1 Production network with supply bottlenecks

This section presents a simple static production network model following a long literature, with only one production chain and variable labor supply (Acemoglu et al., 2012; Carvalho et al., 2021). The key assumption for identification in the empirical model is a negative response of transportation costs to input production shocks. This result is obtained under two not very rigid assumptions. First, a supply rigidity in transportation services, which shuts down a reallocation channel well-known in the production network literature (Carvalho and Tahbaz-Salehi, 2019). Second, a production complementarity between transportation

*Email: moaz.elsayed(at)banque-france.fr
‡Email: christoph.grossesteffen(at)banque-france.fr
§Email: magali.marx(at)banque-france.fr

and an intermediate good. A parameterized version leads to model predictions consistent with our sign restrictions for identification. All model equations are derived below.

Figure A.1: Production chain

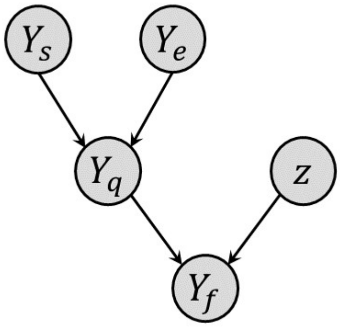

Notes: The arrows indicate the direction of input flows through the production chain. Transportation services, Y_s, and essential intermediate inputs, Y_e, are combined to produce the composite intermediate good, Y_q, and are gross complements. Transportation capacity is fixed in the short run, limiting the reallocation of resources toward transportation services following a shock. Final output, Y_f, is produced using Y_q and delivery time, z, which are gross substitutes. In the empirical SVAR, P_s, z, and Y_f correspond, respectively, to real transportation costs, supplier delivery time, and world industrial production.

We assume a static, closed economy inhabited by a representative household and four firms that produce in three sequential steps in a single production chain (Fig. A.1). For simplicity, we think of the closed economy as the global economy. Transportation services Y_s are produced with capital goods and a Cobb–Douglas production function. A fixed capital stock encapsulates the idea that transportation capacity is assumed to be highly inelastic in the short run, reflecting bottlenecks in shipping fleets and port infrastructure that limit the rapid expansion of transportation services following a disruption (Brancaccio et al., 2025). Importantly, this shuts down the reallocation channel in response to a productivity shock in the same production chain. Transportation firms maximize profits subject to their production technology and the realization of a Hicks-neutral technology shock A_s that we label as *transportation shock*:

$$\max_{\{K\}} \Pi_s = Y_s P_s - R^k K,$$
$$\text{with} \quad Y_s = A_s K^{1-\alpha_s}.$$

In parallel, an essential good firm produces Y_e using labor input in a Cobb–Douglas production function with variable labor input and technology shock A_e that we label as *input production shock*. The firm sells products at a price P_e, leading to a standard optimization problem

$$\max_{\{L\}} \Pi_e = Y_e P_e - WL,$$
$$\text{with} \quad Y_e = A_e L^{\alpha_e}.$$

At a second step, firms combine transportation services and essential goods to produce an intermediate good Y_q with a constant elasticity of substitution (CES) production function, where parameter φ weights input factors for Y_q. This production step is characterized by production complementarity, governed by parameter $1 > \nu$. Thus, there is one bottleneck, the availability of intermediate goods, which is governed by two different sources that enter the CES-production function:

$$\begin{aligned}
\Pi_q &= P_q Y_q - P_s Y_s - P_e Y_e, \\
Y_q &= A_q \left[\varphi Y_s^{\frac{\nu-1}{\nu}} + (1-\varphi) Y_e^{\frac{\nu-1}{\nu}} \right]^{\frac{\nu}{\nu-1}}.
\end{aligned}$$

In a third step, final good producers assemble Y_f using intermediate goods Y_q and (delivery) time z in a CES production function. The use of time captures the possibility to draw on inventories, which leads us to assume a high degree of substitutability between Y_q and z, or $\phi > 1$. The use of time is subject to *ad hoc* adjustment costs $\tau(z)$ with cost parameters κ and η. In the model, the more z is used, the longer it takes final good producers to deliver the good to the consumer. Formally, the firm problem takes the form

$$\begin{aligned}
\Pi_f &= P_f Y_f - P_q Y_q - \tau(z), \\
Y_f &= A_f \left[\omega Y_q^{\frac{\phi-1}{\phi}} + (1-\omega) z^{\frac{\phi-1}{\phi}} \right]^{\frac{\phi}{\phi-1}}, \\
\tau(z) &= \kappa z^{\eta+1}.
\end{aligned}$$

A representative household derives utility from consumption and leisure, and supplies labor to essential good producers in return for a real wage W. Households own the capital stock of transportation firms and receive the return on capital R^k. Given the static setup, there is no intertemporal savings decision and the household's margin of adjusting consumption is the labor-supply decision.

A.2 Equilibrium conditions and first-order conditions

Optimization of essential good producers:

$$\begin{aligned}
\max_{\{L\}} \Pi_e &= Y_e P_e - WL \\
\text{with} \quad Y_e &= A_e L^{\alpha_e}
\end{aligned}$$

F.O.C.

$$W = \alpha_e P_e A_e L_e^{\alpha_e - 1} = \alpha_e P_e A_e^{1/\alpha_e} Y_e^{1-1/\alpha_e}.$$

Optimization of transportation firms:

$$\max_{\{K\}} \Pi_s = Y_s P_s - R^k K$$
$$\text{with} \quad Y_s = A_s K^{1-\alpha_s}$$

F.O.C.

$$R^k = (1-\alpha_s) P_s A_s K^{-\alpha_s}.$$

Optimization of intermediate good firm:

$$\text{From} \quad \Pi_q = P_q Y_q - P_s Y_s - P_e Y_e$$
$$\text{with technology} \quad Y_q = A_q \left[\varphi Y_s^{\frac{\nu-1}{\nu}} + (1-\varphi) Y_e^{\frac{\nu-1}{\nu}} \right]^{\frac{\nu}{\nu-1}}$$

F.O.C.

$$\begin{aligned} \partial Y_s : \quad & P_q A_q \left[\varphi Y_s^{\frac{\nu-1}{\nu}} + (1-\varphi) Y_e^{\frac{\nu-1}{\nu}} \right]^{\frac{1}{\nu-1}} \varphi Y_s^{-1/\nu} - P_s = 0 \\ \Leftrightarrow \quad & P_q A_q \left(\frac{Y_q}{A_q} \right)^{1/\nu} \varphi Y_s^{-1/\nu} - P_s = 0 \\ \Leftrightarrow \quad & \varphi P_q A_q^{1-1/\nu} Y_q^{1/\nu} = P_s Y_s^{1/\nu} \end{aligned}$$

$$\begin{aligned} \partial Y_e : \quad & P_q A_q \left[\varphi Y_s^{\frac{\nu-1}{\nu}} + (1-\varphi) Y_e^{\frac{\nu-1}{\nu}} \right]^{\frac{1}{\nu-1}} (1-\varphi) Y_e^{-1/\nu} - P_e = 0 \\ \Leftrightarrow \quad & P_q A_q \left(\frac{Y_q}{A_q} \right)^{1/\nu} (1-\varphi) Y_e^{-1/\nu} - P_e = 0 \\ \Leftrightarrow \quad & (1-\varphi) P_q A_q^{1-1/\nu} Y_q^{1/\nu} = P_e Y_e^{1/\nu} \end{aligned}$$

thus

$$\begin{aligned} \frac{P_s Y_s^{1/\nu}}{\varphi} &= \frac{P_e Y_e^{1/\nu}}{1-\varphi} \\ \Leftrightarrow \quad Y_e &= \left[\frac{(1-\varphi) P_s Y_s^{1/\nu}}{P_e} \right]^{\nu}. \end{aligned}$$

Optimization of final good firm:

$$\Pi_f = P_f Y_f - P_q Y_q - \tau(z)$$
$$\text{with} \qquad Y_f = A_f \left[\omega Y_q^{\frac{\phi-1}{\phi}} + (1-\omega) z^{\frac{\phi-1}{\phi}} \right]^{\frac{\phi}{\phi-1}}$$
$$\text{and} \qquad \tau(z) = \kappa z^{\eta+1}$$

F.O.C.

$$\begin{aligned}
\partial Y_q: \quad & P_f A_f \left[\omega Y_q^{\frac{\phi-1}{\phi}} + (1-\omega) z^{\frac{\phi-1}{\phi}}\right]^{\frac{1}{\phi-1}} \omega Y_q^{-1/\phi} - P_q = 0 \\
\Leftrightarrow \quad & P_f A_f \left(\frac{Y_f}{A_f}\right)^{1/\phi} \omega Y_q^{-1/\phi} - P_q = 0 \\
\Leftrightarrow \quad & \omega P_f A_f^{1-1/\phi} Y_f^{1/\phi} = P_q Y_q^{1/\phi}
\end{aligned}$$

$$\begin{aligned}
\partial z: \quad & P_f A_f \left[\omega Y_q^{\frac{\phi-1}{\phi}} + (1-\omega) z^{\frac{\phi-1}{\phi}}\right]^{\frac{1}{\phi-1}} (1-\omega) z^{-\frac{1}{\phi}} - (\eta+1)\kappa z^{\eta} = 0 \\
\Leftrightarrow \quad & (1-\omega) P_f A_f \left(\frac{Y_f}{A_f}\right)^{1/\phi} = (\eta+1)\kappa z^{\eta} \\
\Leftrightarrow \quad & (1-\omega) P_f A_f^{1-1/\phi} Y_f^{1/\phi} = (\eta+1)\kappa z^{\eta+1/\phi}
\end{aligned}$$

thus

$$\frac{P_q Y_q^{1/\phi}}{\omega} = \frac{(\eta+1)\kappa z^{\eta+1/\phi}}{1-\omega} \qquad \Rightarrow \qquad z = \left(\frac{(1-\omega) P_q Y_q^{1/\phi}}{\omega(\eta+1)\kappa}\right)^{\frac{1}{\eta+1/\phi}}.$$

Optimization of households:

$$\begin{aligned}
& U(C) - \Phi(L), \\
\text{with} \quad & U(C) = \frac{C^{1-\sigma}}{1-\sigma}, \quad \Phi(L) = \alpha \frac{L^{1-\gamma}}{1-\gamma}, \\
\text{s.t.} \quad & WL + R^k K + E = P_f C.
\end{aligned}$$

F.O.C.

$$\partial C: \quad C^{-\sigma} = \lambda P_f, \qquad \partial L: \quad \theta L^{-\gamma} = \lambda W,$$

combining to eliminate λ,

$$\theta L^{-\gamma} = C^{-\sigma} \frac{W}{P_f}.$$

A.3 Parameterization

A.4 Comparative statics and prices

The comparative statics verify that the parameterization reproduces the qualitative sign restrictions imposed in the empirical model. Tab. A.2 shows the comparative-static changes of equilibrium allocations in the case of the two sectoral supply shocks, while Fig. A.3 illustrates the implications for supply, demand, and equilibrium allocations and prices on the four product markets of the model. First, consider a transportation shock by a decline

Table A.1: Parameterization

Parameter	value	comment
α_e	0.33	labor share, essential goods
$1-\alpha_s$	0.9	capital share, transportation services
K	0.65	capital stock, transportation services
φ	0.5	weight transportation good in intermediate good
ν	0.5	production complementarity (Y_s, Y_e)
ω	0.8	weight intermediate good in final good
ϕ	10	substitutability (Y_q, z)
κ	0.75	param. 1, time adjustment cost
η	50	param. 2, time adjustment cost
θ	2	scaling labor supply
σ	2	risk aversion
γ	0.455	labor elasticity

Figure A.2: Isoquants of production technologies

(a) Intermediate good production

(b) Final good production

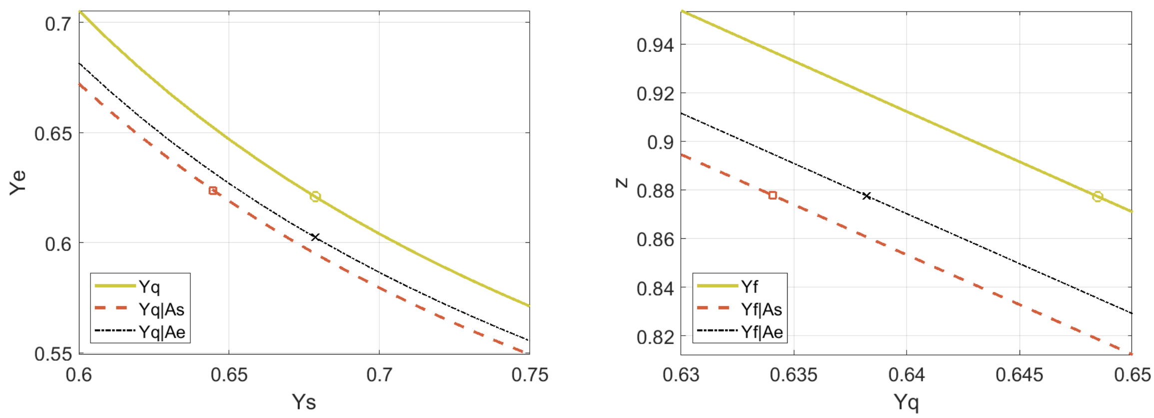

Notes: Isoquants of production functions derived from the model, based on the parameterization in Tab. A.1. The transportation shock is modeled as a decline in productivity A_s by 5 percent. In analogy, the production bottleneck shock is modeled as a decline in productivity A_e by 5 percent.

in the productivity parameter A_s by 5 percent. Supply of Y_s shifts to the left, leading to an increase in transportation costs P_s, which is only partly offset by an increase of essential goods production Y_e given the production complementarity. Production of intermediate goods Y_q drops due to a downstream output effect, leading to rising producer prices P_q. High substitutability leads to an increase of delivery time z. Adjustment costs prevent that the shock on production is fully offset, leading to shifts in supply and demand of final goods Y_f at higher equilibrium prices and lower quantities.

Let us turn next to the input production shock, a drop in A_e by 5 percent. While there is an imminent drop in supply of Y_e goods, the fixed capacity of transportation services in conjunction with production complementarity and market clearing leads to a drop in the

Table A.2: Model responses to supply bottleneck shocks

	Y_f	z	P_s	P_q	P_f
transportation	-1.66% (−)	0.06% (+)	9.18% (+)	3.06% (+)	3.00% (.)
production	-1.18% (−)	0.03% (+)	-1.60% (−)	1.57% (+)	1.53% (.)

Notes: Responses are reported as percentage changes between equilibrium allocations without shocks, i.e. $A_s = A_e = 1$, and allocations under a shock occurrence. The transportation shock is modeled as a decline in productivity A_s by 5 percent. In analogy, the input production shock is captured by a decline in productivity A_e by 5 percent. Assumptions used for sign restrictions in the empirical model are reported in parentheses.

price for transportation services P_s. A negative downstream output effect on Y_q is again partially offset by recourse to z, increasing delivery time. Overall, final good prices P_f rise and output Y_f drops.

Note that the model predicts a higher magnitude of the transportation shock on producer prices P_q and consumer prices P_f. This is due to the different production technologies in the transportation and essential goods sectors.

Figure A.3: Sectoral supply shocks in the model

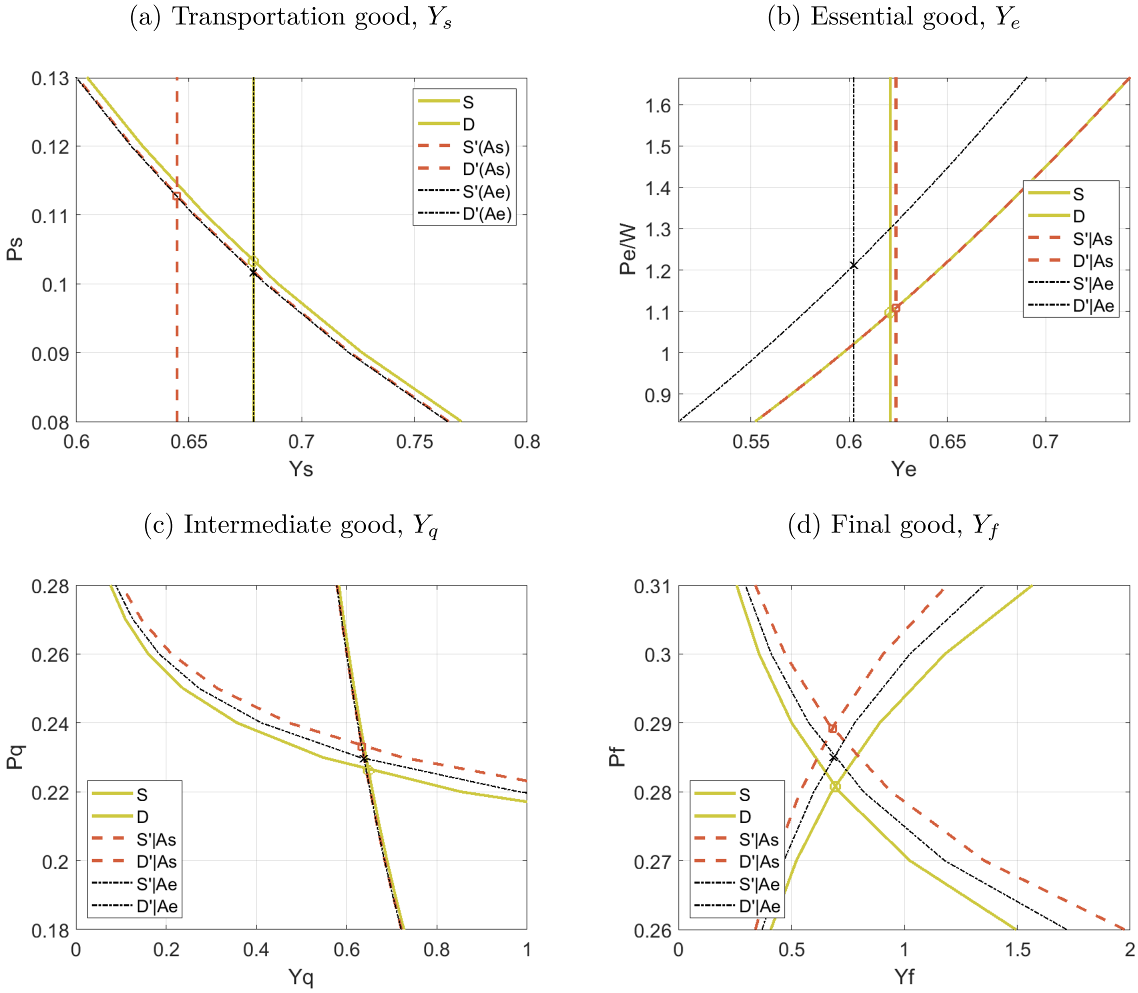

Notes: Supply and demand schedules derived from the model, based on the parameterization in Tab. A.1. The transportation shock is modeled as a decline in productivity A_s by 5 percent. In analogy, the input production shock is modeled as a decline in productivity A_e by 5 percent.

B Data

B.1 Data sources

B.1.1 Global variables

This section describes in detail the variables entering the baseline specification. Fig. B.1 shows the three variables that enter the supply-chain VAR in their respective transformations.

World industrial production. The world industrial production index follows Baumeister and Hamilton (2019). It is constructed from industrial production indices for OECD countries and six major non-member economies (Brazil, China, India, Indonesia, Russia, and South Africa), aggregated using IMF GDP weights. The series is retrieved from Christiane Baumeister's personal website.

Figure B.1: Global series entering supply-chain VAR

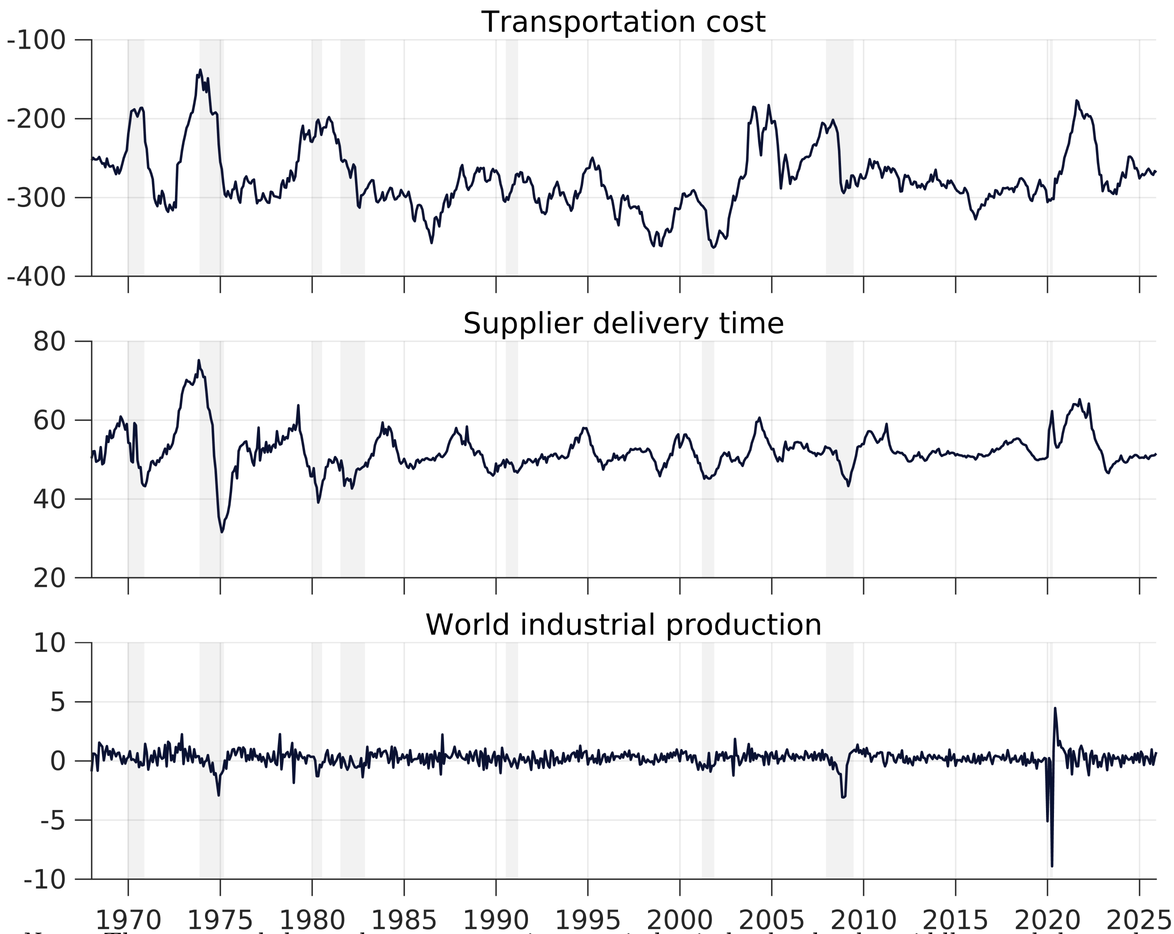

Notes: The top panel shows the transportation-cost index in log levels, the middle panel shows the supplier-delivery-time index in levels, and the bottom panel shows the monthly change in the log of world industrial production, expressed in percentage points. Shaded areas mark NBER-dated U.S. recessions.

Supplier delivery times. Supplier delivery times are measured using the J.P. Morgan Global Manufacturing PMI Suppliers' Delivery Times Index, compiled by S&P Global Market Intelligence, and retrieved via Bloomberg (series code PMI/GL/MAN/SD). The series is available from January 1998 onwards and is back-cast to January 1968 using the ISM Manufacturing Supplier Deliveries Index, retrieved via Bloomberg (series code NAPMSUPL Index). The back casting procedure follows a linear fitted model:

$$globalPMI_t - 50 = \alpha + \beta \times (ISMmanufSDT_t - 50) + \varepsilon_t$$

Transportation costs. The transportation-cost index is based on Hamilton (2019). It combines various nominal indices of transportation cost in maritime shipping for bulk freight and containers, complemented by air freight rates, ax detailed in Appendix B.1.2. Series are converted in real terms using U.S. CPI inflation. Appendix B.2 explains all steps in the construction of the index.

B.1.2 Transportation cost series

Baltic Dry Index. The Baltic Dry Index (BDI) is published by the Baltic Exchange and measures the cost of shipping major dry bulk commodities, including iron ore, coal, and grain, across international maritime routes. It is a composite index based on freight rates for several classes of dry bulk vessels. The index is available on a daily basis from January 1985 onwards. We use monthly averages of the daily observations retrieved from Bloomberg (series code $BDIYIndex$).

HARPEX. The Harper Petersen Charter Rates Index (HARPEX) is published by Harper Petersen & Co. and measures charter rates for container vessels across different ship-size categories. As a composite index of container ship charter rates, it captures conditions in the container shipping market. The index is available on a weekly basis from January 2004 onwards. We use monthly averages of the weekly observations retrieved from Thompson Reuters (series code $HARPEXI$).

Drewry World Container Index. The Drewry World Container Index (WCI) is published by Drewry Shipping Consultants and measures spot freight rates for 40-foot containers across the world's major east–west trade routes. As a composite index of container freight rates, it captures conditions in the global container shipping market and provides a broad measure of international container transportation costs. The index is available on a weekly basis from June 2011 onwards. We use monthly averages of the weekly observations retrieved from Bloomberg (series code $WCIDCOMPIndex$).

New ConTex. The New ConTex (Container Ship Time Charter Assessment Index) is published by the Association of Hamburg and Bremen Shipbrokers (VHBS) and measures time charter rates for container vessels across representative ship-size categories. The index is available on a twice-weekly basis from October 2007 onwards. We use monthly averages of the published observations retrieved from Bloomberg (series code $CTEXIDEXIndex$).

Air freight price indices. The Inbound Price Index (International Services): Air Freight and the Outbound Price Index (International Services): Air Freight are published by the U.S. Bureau of Labor Statistics (BLS) as part of the U.S. Import and Export Price Index program. The indices measure changes in the prices of international air freight transportation services for shipments entering and leaving the United States, respectively, and provide indicators of developments in global air transportation costs. The indices are available on a monthly basis from September 1990 onwards. We retrieve the not seasonally adjusted series from FRED, Federal Reserve Bank of St. Louis (series codes $IC131$ and $IS231$).

Consumer price inflation. Consumer price inflation is measured by the Consumer Price Index for All Urban Consumers: All Items in U.S. City Average (CPI-U), published by the U.S. Bureau of Labor Statistics (BLS). The series is seasonally adjusted and available on a monthly basis from January 1947 onwards. We retrieve the data from FRED, Federal Reserve Bank of St. Louis (series code CPIAUCSL).

B.1.3 U.S. block variables

Headline inflation. We use the price index for personal consumption expenditures as provided by the U.S. Bureau of Economic Analysis, retrieved from FRED, Federal Reserve Bank of St. Louis (series code $PCEPI$).

Core inflation. We use the index for personal consumption expenditures excluding food and energy as provided by the U.S. Bureau of Economic Analysis, retrieved from FRED, Federal Reserve Bank of St. Louis (series code PCEPILFE).

Services inflation. Services inflation is measured by the PCE index for services excluding energy and housing provided by the U.S. Bureau of Labor Statistics. The series is seasonally adjusted and retrieved from FRED, Federal Reserve Bank of St. Louis (series code IA001260M).

Producer price inflation. We use the producer price index by commodity for all commodities as provided by the U.S. Bureau of Labor Statistics, retrieved from FRED, Federal Reserve Bank of St. Louis (series code PPIACO).

U.S. industrial production. We use the Federal Reserve's monthly index of industrial production, which covers manufacturing, mining, and electric and gas utilities. The series is seasonally adjusted and retrieved from FRED, Federal Reserve Bank of St. Louis (series code INDPRO).

Unemployment rate. We use unemployment rate as provided by the U.S. Burea of Labor Statistics. The series is seasonally adjusted and retrieved from FRED, Federal Reserve Bank of St. Louis (series code UNRATE).

Manufacturing inventories. We use real manufacturing and trade inventories as constructed by the Federal Reserve Bank of St. Louis based on data from the U.S. Bureau of Economic Analysis. The series is seasonally adjusted and retrieved from FRED, Federal Reserve Bank of St. Louis (series code INVHMRMT).

1-year interest rate. We use the market yield on U.S. Treasury securities at 1-year constant maturity and quoted on an investment basis from the Board of Governors of the Federal Reserve System, retrieved from FRED, Federal Reserve Bank of St. Louis (series code DGS1).

B.1.4 Other data

Real oil price. We use the real U.S. refiners' imported acquisition cost (IRAC) for crude oil, obtained from the U.S. Energy Information Administration (EIA). Since the IRAC series begins only in January 1974, we extend it backwards with the monthly West Texas Intermediate (WTI) crude oil price prior to 1974, retrieved from FRED, Federal Reserve Bank of St. Louis (series code WTISPLC). The nominal series is deflated by the U.S. consumer price index to obtain a consistent monthly measure of the real price of oil over the full sample.

B.2 Transportation cost index

Figure B.2 shows the transportation cost index. We combine monthly information from shipping and air-freight markets—BDI, HARPEX, the Drewry World Container Index (composite), ConTex, and the BLS inbound/outbound air-freight indices—together with the nominal Kilian shipping index (1968:1–2007:12) as reconstructed by Hamilton (2019). Appendix B.1.2 provides a description of all series and data sources. For each price series $p_{i,t}$ we first normalize to its 2018 average,

$$\tilde{p}_{i,t} \;=\; 100 \cdot \frac{p_{i,t}}{\overline{p}_{i,2018}},$$

and compute monthly log growth $g_{i,t} = \Delta \log \tilde{p}_{i,t}$ (which is equivalent to $\Delta \log p_{i,t}$). For the Kilian nominal shipping index we use its monthly first difference $g_t^{\mathrm{KH}} = \Delta \mathrm{knom}_t$ as an additional growth series over its available span. The composite growth rate is the unweighted average across all available series in month t,

$$g_t \;=\; \frac{1}{N_t} \sum_{i \in \mathcal{I}_t} g_{i,t},$$

Figure B.2: Transportation cost index

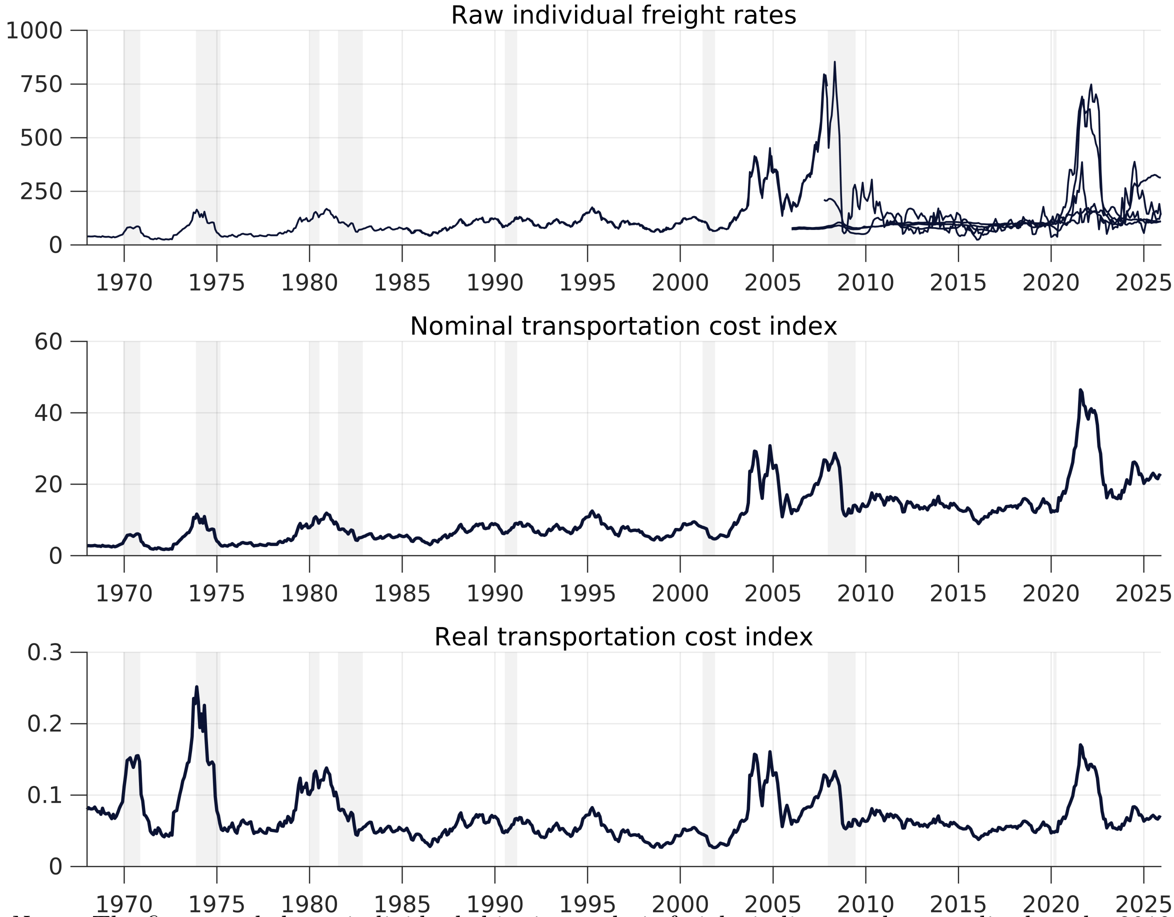

Notes: The first panel shows individual shipping and air-freight indices, each normalized to the 2018 average (=100): Baltic Dry Index (BDI), HARPEX, Drewry World Container Index (composite), ConTex (container ship time charter), and BLS inbound/outbound air-freight price indices. The second panel shows the resulting nominal transportation index (1968:1=1). The third panel reports the index in real terms after deflation by U.S. CPI. The sample starts in 1968:1 and extends through 2025:6.

where $\mathcal{I}_t$ is the set of non-missing series and $N_t = |\mathcal{I}_t|$. We initialize the composite log level at $x_{1968:1} = 1$ and cumulate growth to obtain the nominal log index,

$$x_t \;=\; x_{t-1} + g_t,$$

then exponentiate $T_t^N = \exp(x_t)$. To obtain the real index we subtract the log of U.S. CPI, $x_t^R = x_t - \log(\mathrm{CPI}_t)$, which is equivalent to deflating the nominal level, $T_t^R = T_t^N/\mathrm{CPI}_t$.

C Additional results

This section provides additional empirical results that complement the main analysis. Appendix C.1 discusses the historical series of structural shocks. Appendix C.2 provides the evolution of all GSTIX indicators including the robust credible set. Appendix C.3 presents the propagation of a congestion shock in global supply chains to U.S. data.

C.1 Historical evolution of shocks

Fig. C.1 reports posterior summaries of the identified monthly structural shocks. Three remarks are useful for their interpretation. First, the posterior-mean series shown in the figure averages, at each date, structural shocks across the set of admissible models and therefore does not correspond to the sequence of structural innovations from any single accepted draw. For each accepted draw, serially uncorrelated structural innovations are a maintained implication of the VAR specification; this property need not carry over to posterior means taken across different structural models. Serial correlation in the posterior-mean series should therefore not by itself be interpreted as evidence of VAR misspecification.

Second, narrative events do not mechanically imply large structural shocks. Narrative restrictions discipline the economic interpretation of selected disturbances, while their magnitude is determined jointly by the data and the remaining identifying restrictions. Accordingly, some narrative episodes highlighted by the vertical bars in Fig. C.1 generate only modest innovations, while sizeable shocks also occur outside the narrative sample. The discussion below therefore focuses selectively on prominent historical episodes that were not used as narrative restrictions and can serve as external checks on the economic interpretation of the recovered shocks.

Third, the posterior-mean series display distinct historical patterns and are rarely simultaneously large. This provides additional evidence that the identification separates different sources of global supply-chain tensions rather than merely capturing periods of generally elevated supply-chain stress.

Transportation shocks display several sizeable realizations outside the narrative episodes used for identification. A pronounced positive shock in November 1971 coincides with major U.S. dock strikes that disrupted port operations and international shipping. Another cluster of positive shocks appears in 2004, during a period of exceptionally strong growth in world trade and tight transportation capacity. The positive realization in August 2021 similarly coincides with the height of pandemic-related stress in global shipping: the port-congestion measure of Bai et al. (2026) show a peak around mid-2021.

Input-production shocks also line up with major production disruptions that are not used for narrative identification. Positive shocks already emerge in January and February 2020, when the initial Covid-19 outbreak disrupted manufacturing activity and input supply in China, followed by an exceptionally large positive innovation in April as shutdowns became global. The sequence reverses sharply between May and July as production restarted, consistent with the shocks capturing unexpected changes in production conditions rather than the persistence of shortages themselves. A further positive innovation in April 2022 coincides with renewed factory closures and supply-chain disruptions associated with lockdowns in China. An earlier positive realization in November 1973 coincides with widespread shortages of industrial inputs. Contemporaneous Federal Reserve reports document rationing and

Figure C.1: Historical evolution of supply shocks

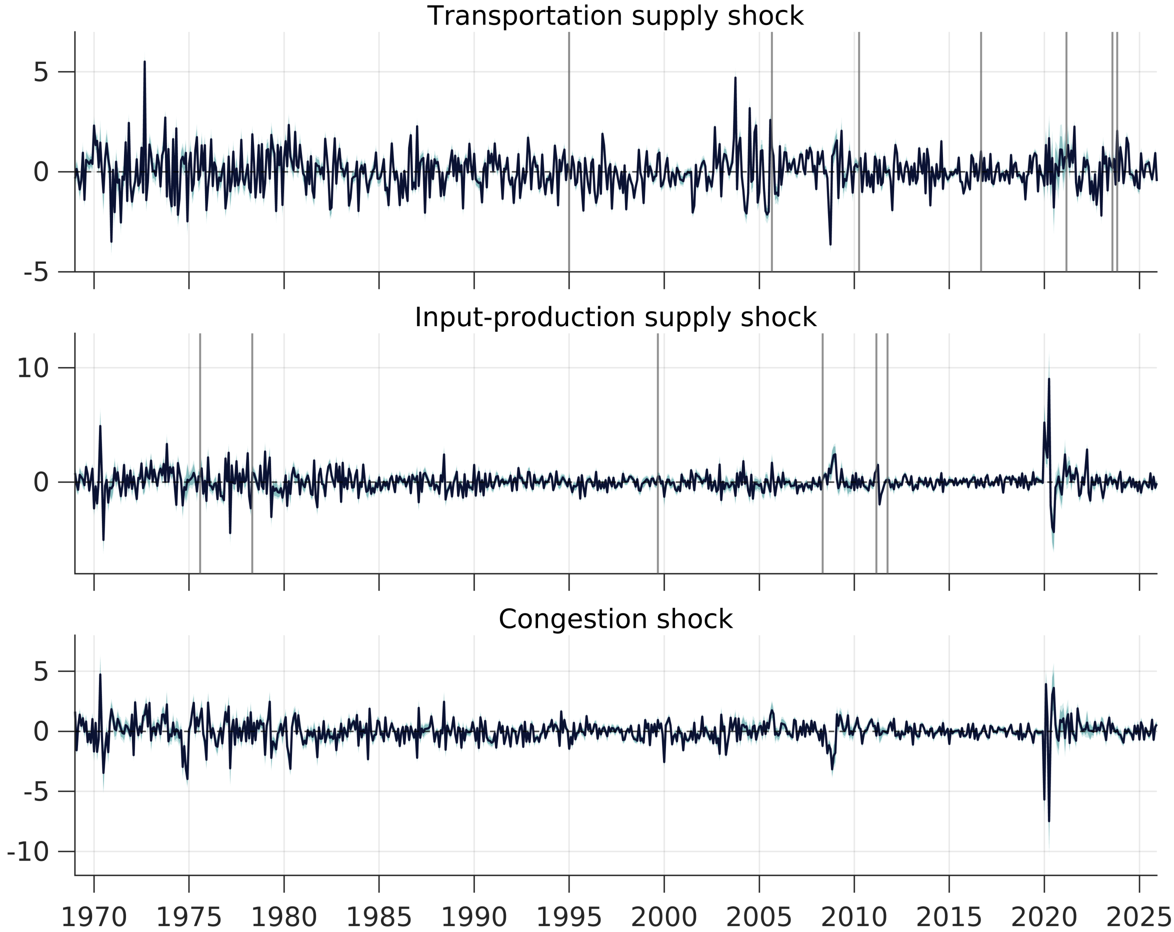

Notes: Monthly posterior means (solid lines) and 68% and 90% robust credible regions (dark and light shaded areas) for the identified structural shocks. Vertical lines indicate the narrative episodes used in the identifying restrictions. Narrative restrictions determine the economic interpretation of selected shocks but do not impose their magnitude, which is estimated jointly from the data and the remaining identifying restrictions.

severe shortages of metals, steel products, paper, and other raw and semi-finished materials, in some cases resulting in production stoppages and layoffs (Federal Reserve System, 1973). While these shortages were partly intertwined with the emerging energy crisis, the reports explicitly describe broader materials scarcity beyond energy products.

Congestion shocks align closely with major fluctuations in global activity, despite no historical episodes being used to identify this shock. Negative realizations cluster during the global slowdown of 1974 and the collapse in world demand during the Global Financial Crisis. The strongest pattern occurs around the Covid-19 pandemic: an exceptionally large negative congestion shock accompanies the collapse in global activity in early 2020, followed by large positive innovations in June and July as demand rebounded rapidly relative to available production and transportation capacity.

C.2 Global supply chain tension indices

Figure C.2: Transport and input-production tensions

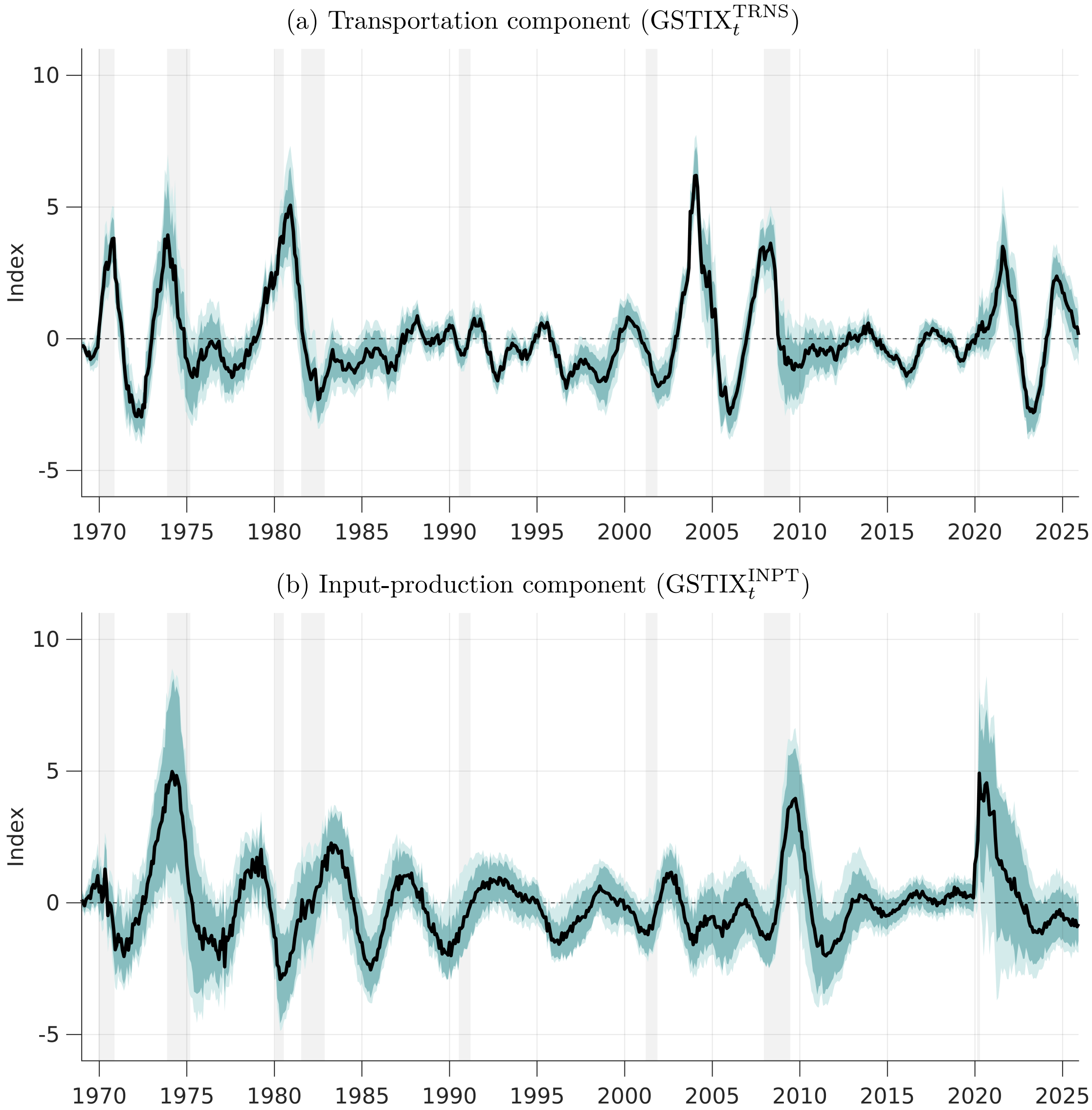

Notes: Monthly measures of supply-side global supply-chain tensions constructed from the historical decomposition of the baseline SVAR. Panel (a) reports the transportation component, $\mathrm{GSTIX}_t^{\mathrm{TRNS}}$, which measures tensions attributable to transportation shocks. Panel (b) reports the input-production component, $\mathrm{GSTIX}_t^{\mathrm{INPT}}$, which measures tensions attributable to input-production shocks. The two components sum to the composite Global Supply Chain Tension Index, $\mathrm{GSTIX}_t^{\mathrm{COMP}}$. Solid lines denote posterior means; dark and light shaded areas denote the 68% and 90% robust credible regions, respectively. Vertical grey bars indicate NBER U.S. recessions.

Fig. C.3 compares the composite GSTIX with three alternative measures of supply-chain stress. Despite substantial differences in construction, the indices display pronounced co-movement during major disruption episodes. The GSTIX and the U.S. Shortage Index of Caldara et al. (2025) rise sharply during the supply disruptions of the 1970s, while all available measures indicate exceptionally elevated tensions during the pandemic. The timing and magnitude of individual peaks nevertheless differ. In particular, the GSCPI of Benigno et al. (2022) peaks in late 2021, while the newspaper-based measures remain particularly elevated into 2022. These differences are consistent with their distinct information sets: the GSCPI combines transportation costs and manufacturing indicators after attempting to purge demand effects, the U.S. Supply Bottlenecks Index of Burriel et al. (2024) measures newspaper reporting on supply-chain disruptions, and the broader Shortage Index captures reported shortages of industrial goods, energy, food, and labor. GSTIX instead measures the dynamic historical contribution of structurally identified transportation and input-production shocks to transportation costs and supplier delivery times.

Figure C.3: GSTIX and alternative measures of supply-chain stress

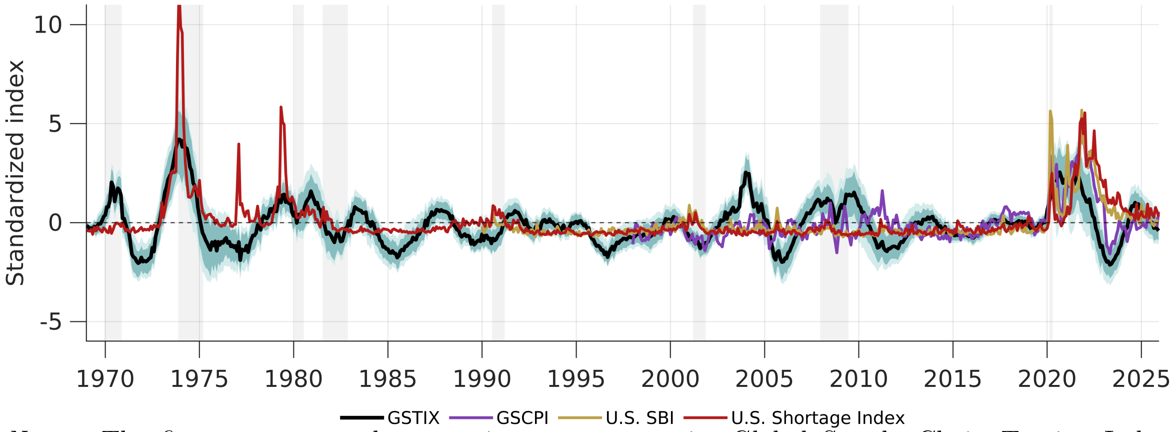

Notes: The figure compares the posterior-mean composite Global Supply Chain Tension Index (GSTIX) with the Global Supply Chain Pressure Index (GSCPI) of Benigno et al. (2022), the U.S. Supply Bottlenecks Index (SBI) of Burriel et al. (2024), and the U.S. Shortage Index of Caldara et al. (2025). For comparability, all four series are standardized to have mean zero and unit standard deviation over the common sample beginning in 1998, defined by the availability of the GSCPI; the displayed sample starts in January 1969, corresponding to the beginning of the GSTIX sample. The solid black line denotes the posterior mean of the GSTIX; dark and light shaded areas indicate the 68% and 90% robust credible regions, respectively. Vertical shaded bars indicate NBER U.S. recessions.

Table C.1: Correlation with alternative measures of supply-chain stress

	GSTIX	GSTIX + GSCIX
GSCPI (Benigno et al., 2022)	0.495	0.718
U.S. Supply Bottlenecks Index (Burriel et al., 2024)	0.321	0.509
U.S. Shortage Index (Caldara et al., 2025)	0.196	0.487

Notes: The table reports pairwise correlations over the common sample 1998M1–2025M12. The first column reports correlations with the composite supply-side GSTIX. The second column reports correlations with the sum of the composite GSTIX and the Global Supply Chain Congestion Index (GSCIX).

C.3 Propagation of congestion shock to U.S. data

This section reports impulse responses of the congestion shock in the block-exogenous VAR. Unlike the two supply-side disturbances discussed in the main text, the congestion shock captures periods in which expansions in global activity strain existing production and transportation capacity. The resulting responses therefore illustrate how activity-driven congestion tensions propagate to U.S. activity, inflation, and monetary policy.

Figure C.4: IRFs of congestion shock (U.S. data)

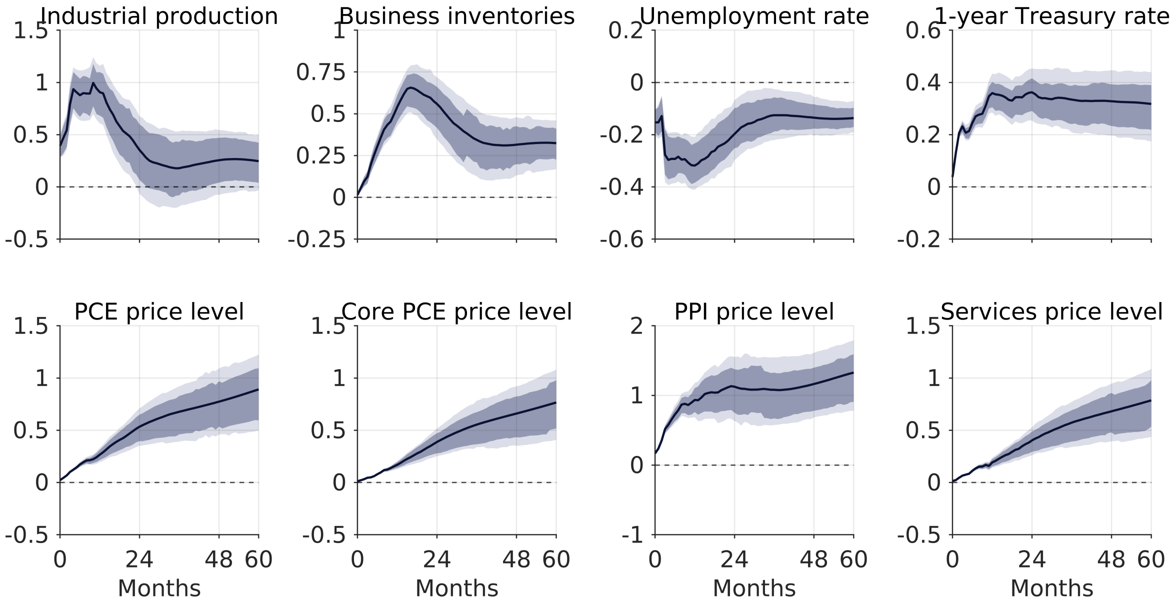

Notes: Impulse responses to a one-standard-deviation congestion shock in the block-exogenous VAR. Dark and light shaded areas denote the 68% and 90% robust credible regions, respectively. Responses for industrial production, business inventories, PCE, core PCE, PPI, and services prices are reported in cumulative form and should be interpreted as percentage deviations from the pre-shock level. Responses of the unemployment rate and the one-year Treasury rate are measured in percentage points.

The congestion shock exhibits markedly different transmission from the two adverse supply-side disturbances discussed in the main text. Industrial production expands immediately and remains above baseline throughout the horizon, while unemployment falls persistently. Business inventories increase strongly during the first two years before stabilizing at an elevated level, consistent with firms expanding production and rebuilding inventories in response to strong demand.

Inflation rises broadly across all price measures. Producer prices respond rapidly, while PCE, core PCE, and services prices increase more gradually and persistently, reflecting the pass-through of capacity pressures to consumer prices. In response to stronger activity and sustained inflation, the one-year Treasury rate increases persistently by roughly 30 basis points.

Overall, the responses support the interpretation of the congestion shock as a activity-driven disturbance operating through capacity constraints rather than an adverse supply disruption. Although congestion raises transportation costs and supplier delivery times in the global block, its macroeconomic consequences differ fundamentally from those of transportation and input-production shocks: output expands rather than contracts, inventories accumulate rather than decline, and inflation reflects strong aggregate activity interacting with limited production and logistics capacity.

D Discussion of narrative events

D.1 Transportation events

[1] **January 1995** corresponds to the **Great Hanshin earthquake** of 17 January 1995, which caused severe damage to the Port of Kobe, then Japan's sixth-largest container port and the principal maritime gateway to the Kansai region. Quay-wall failures caused by soil liquefaction, collapsed container cranes, and widespread berth damage rendered much of the port inoperable, leading to a sharp disruption of maritime freight traffic and the rerouting of cargo to other ports (Chang, 2000). Although port facilities were largely reconstructed within two years, the immediate impact was a substantial disruption to transportation infrastructure rather than production capacity (Hiroshi and Hsiao, 2015).

[2] **September 2005** captures **Hurricane Katrina (USA)**, which severely disrupted maritime transportation along the U.S. Gulf Coast. Damage to ports, navigation channels, and connecting transport infrastructure temporarily impaired traffic through the Lower Mississippi River, an important gateway for U.S. bulk commodity exports. Using port-level trade data, Friedt (2021) documents large trade reductions at directly affected ports by about 95% one month after landfall, together with substantial rerouting of cargo to neighboring ports.

[3] **April 2010** marks the eruption of **Iceland's Eyjafjökull volcano**. The resulting volcanic ash plume forced the closure of much of European airspace for eight days, cancelling about 107,000 flights. Exploiting this disruption as a natural experiment, Besedeša and Murshid (2018) show that average flight cancellations of around 50% reduced U.S. imports from affected European countries by 10.9–21.8% and Japanese imports by 11.9–27.5%, while shipments by sea remained unaffected.

[4] **September 2016** refers to the unexpected bankruptcy of **Hanjin Shipping (South Korea)**, then the world's seventh-largest container carrier. The bankruptcy stranded approximately $17.5 billion of cargo in transit as ports and terminal operators refused to service Hanjin vessels, leaving ships at anchor and disrupting container movements across global shipping networks (Notteboom et al., 2021). Exploiting this event as an exogenous disruption to international shipping, Kwon (2021) shows that the resulting delays propagated through global supply chains, providing a clear example of a transportation shock.

[5] **March 2021** corresponds to the grounding of the container ship *Ever Given* in the **Suez Canal (Egypt)**, which blocked one of the world's busiest maritime trade routes for six

consecutive days (23–29 March) and created a backlog of hundreds of vessels (Tran et al., 2025). The disruption delayed at least 25 container ships carrying more than 217,000 TEUs to U.S. East Coast ports (BTS, 2021).

[6] **August 2023** denotes a **Panama Canal** incident in response to a prolonged drought, as water levels in Gatún Lake dropped to an extent that locks could no longer be operated at usual frequency. The port authority limited daily transits and required ships to lighten their load. As a consequence, Chico et al. (2024) identified more than 290 vessels that were forced to take alternative transit routes, usually longer, leading to higher transportation costs and shipping delays.

[7] **November 2023** marks the onset of Houthi attacks from Yemen on commercial vessels in the **Red Sea**, an abrupt geopolitical disruption that prompted major carriers to suspend passages through the Bab-el-Mandeb Strait and reroute around the Cape of Good Hope. Between 1 November 2023 and 28 February 2024, vessel transits through the strait declined by 55%, while rerouting added between 8 and 17 days to voyages (ITF-OECD, 2024). By lengthening vessel rotations and absorbing effective shipping capacity, the disruption propagated through global liner networks, affecting sailing schedules, subsequent port calls, and maritime supply chains far beyond the Red Sea, while rerouting was subsequently integrated in plans for inventory orders (Notteboom et al., 2024).

D.2 Input-production events

[8] **August 1975** coincides with the closure of the **Benguela Railway (Angola)** following the outbreak of the Angolan civil war. Although the event disrupted a transportation corridor, the railway primarily served as the principal export route for cobalt and copper from the Katanga region in southern Zaire (now the Democratic Republic of Congo) rather than as part of an integrated global transportation network. Its closure therefore reduced access to a critical production input, sharply constraining global cobalt supply and contributing to substantial price increases for downstream industries reliant on the metal (Habib et al., 2016; Gulley, 2022).

[9] **May 1978** (Shaba II) marks renewed conflict in the **Shaba region of southern Zaire (DR Congo)**, which directly disrupted cobalt mining and processing operations in one of the world's dominant producing regions. The conflict further tightened global cobalt supply and reinforced the shortages and price increases that had begun with the closure of the Benguela export corridor (Habib et al., 2016; Gulley, 2022).

[10] **September 1999** is associated with the **Chi-Chi earthquake (Taiwan)**. Damage to the electricity-transmission network halted production at all 28 wafer fabs in Hsinchu Science Park, despite relatively limited structural damage to the plants themselves. The power interruption destroyed work-in-process and delayed the restart of fabrication lines

through extensive inspection, recalibration, and requalification requirements. Because Taiwanese foundries accounted for roughly two-thirds of global contract chip production, the localized outage temporarily disrupted the supply of a critical intermediate input to electronics producers worldwide (Huang and Hosoe, 2017; Saxenian, 2004).

[11] **May 2008** denotes the **Wenchuan earthquake (China)** in Sichuan Province. The earthquake severely damaged a geographically concentrated cluster of fertilizer, phosphate-processing, chemical, and industrial-equipment producers around Shifang, Deyang, Mianzhu, and Mianyang. Collapsed production buildings, damaged equipment and utilities, and disruptions to phosphate mining caused plant shutdowns lasting up to several months (Krausmann et al., 2010). Because these industries supplied intermediate inputs to manufacturing elsewhere in China, the resulting bottlenecks propagated through interregional supply chains, including to the major manufacturing provinces of Guangdong and Zhejiang (Huang et al., 2022).

[12] **March 2011** denotes the **Tōhoku earthquake (Japan)**, which disrupted the production of specialized intermediate inputs. This well-studied event led to disruptions that propagated upstream and downstream through domestic production networks before transmitting internationally to downstream manufacturers reliant on Japanese suppliers, including firms in the United States (Boehm et al., 2019; Carvalho et al., 2021).

[13] **October 2011** marks the **Thailand floods**, which inundated seven major industrial estates north of Bangkok hosting 804 firms, including 451 Japanese manufacturers, concentrated in the automotive, electronics and hard-disk-drive industries (METI, 2012; Haraguchi and Lall, 2015). Resulting shortages of specialized intermediate inputs propagated through international production networks. Reflecting the severity of these disruptions, prices of major hard-disk drives approximately tripled during the flood period (UNISDR, 2012). Consistent with this mechanism, Forslid and Sanctuary (2023) find that output of Swedish firms exposed to Thai exporters declined by about 8% in 2012.

References

Acemoglu, D., Carvalho, V., Ozdaglar, A., and Tahbaz-Salehi, A. (2012). The network origins of aggregate fluctuations. *Econometrica*, 80(5):1977–2016.

Bai, X., Fernandez-Villaverde, J., Li, Y., and Zanetti, F. (2026). The causal effects of global supply chain disruptions on macroeconomic outcomes: Evidence and theory. *American Economic Review*. Forthcoming.

Baumeister, C. and Hamilton, J. (2019). Structural interpretation of vector autoregressions with incomplete identification: Revisiting the role of oil supply and demand shocks. *American Economic Review*, 109(5):1873–1910.

Benigno, G., di Giovanni, J., Groen, J. J., and Noble, A. I. (2022). The GSCPI: A new barometer of global supply chain pressures. Federal Reserve Bank of New York Staff Papers No. 1017.

Besedeša, T. and Murshid, A. P. (2018). Experimenting with ash: The trade-effects of airspace closures in the aftermath of Eyjafjallajökull. FREIT Working Paper No. 1397.

Boehm, C. E., Flaaen, A., and Pandalai-Nayar, N. (2019). Input linkages and the transmission of shocks: Firm-level evidence from the 2011 Tōhoku earthquake. *Review of Economics and Statistics*, 101(1):60–75.

Brancaccio, G., Kalouptsidi, M., and Papageorgiou, T. (2025). Rigidities in transportation and supply chain disruptions. *AEA Papers and Proceedings*, 115:543–550.

BTS (2021). Suez canal blockage by Ever Given will affect U.S. ports, businesses, consumers. Bureau of Transportation Statistics Data Spotlight.

Burriel, P., Kataryniuk, I., Monero Pérez, C., and Viani, F. (2024). A new supply bottleneck index based on newspaper data. *International Journal of Central Banking*, 20(2):17–67.

Caldara, D., Iacoviello, M., and Yu, D. (2025). Measuring shortages since 1900. Board of Governors of the Federal Reserve System International Finance Discussion Paper No. 1407.

Carvalho, V., Nirei, M., Saito, Y., and Tahbaz-Salehi, A. (2021). Supply chain disruptions: Evidence from the Great East Japan earthquake. *Quarterly Journal of Economics*, 136(2):1255–1321.

Carvalho, V. and Tahbaz-Salehi, A. (2019). Production networks: A primer. *Annual Review of Economics*, 11:635–663.

Chang, S. E. (2000). Disasters and transportation systems: Loss, recovery and competition at the port of Kobe after the 1995 earthquake. *Journal of Transport Geography*, 8(1):53–65.

Chico, C., Wang, Z., Reyes, E. K. C., and Mariasingham, M. J. (2024). AIS-based framework for analyzing the impacts of passageway disruptions. *Economics of Disasters and Climate Change*, 8:489–511.

Federal Reserve System (1973). National summary. Federal Reserve System Working Paper. November 14, 1973.

Forslid, R. and Sanctuary, M. (2023). Climate risks and global value chains: The impact of the 2011 Thailand flood on Swedish firms. CEPR Discussion Paper No. 17855.

Friedt, F. L. (2021). Natural disasters, aggregate trade resilience, and local disruptions: Evidence from Hurricane Katrina. *Review of International Economics*, 29(5):1081–1120.

Gulley, A. L. (2022). One hundred years of cobalt production in the Democratic Republic of the Congo. *Resources Policy*, 79:103007.

Habib, K., Hamelin, L., and Wenzel, H. (2016). A dynamic perspective of the geopolitical supply risk of metals. *Journal of Cleaner Production*, 133:850–858.

Hamilton, J. D. (2019). Measuring global economic activity. *Journal of Applied Econometrics*, 36(3):293–303.

Haraguchi, M. and Lall, U. (2015). Flood risks and impacts: A case study of Thailand's floods in 2011 and research questions for supply chain decision making. *International Journal of Disaster Risk Reduction*, 14:256–272.

Hiroshi, H. and Hsiao, C. (2015). Disentangling the effects of multiple treatments—measuring the net economic impact of the 1995 Great Hanshin-Awaji earthquake. *Journal of Econometrics*, 186(1):66–73.

Huang, M. C. and Hosoe, N. (2017). Fiscal and social costs of recovery programs for an earthquake disaster in northern Taiwan. *Journal of Asian Economics*, 53:1–17.

Huang, R., Malik, A., Lenzen, M., Jin, Y., Wang, Y., Faturay, F., and Zhu, Z. (2022). Supply-chain impact of Sichuan earthquake: A case study using disaster input-output analysis. *Natural Hazards*, 2022(110):2227–2248.

ITF-OECD (2024). The Red Sea crisis: Impacts on global shipping and the case for international co-operation. Background Paper. International Transport Forum, Organisation for Economic Co-operation and Development.

Krausmann, E., Cruz, A. M., and Affeltranger, B. (2010). The impact of the 12 may 2008 Wenchuan earthquake on industrial facilities. *Journal of Loss Prevention in the Process Industries*, 23(2):242–248.

Kwon, C. (2021). Supply chain disruptions and causal outcomes: Evidence from the bankruptcy of Hanjin Shipping. SSRN Working Paper No. 3293272.

METI (2012). White paper on international economy and trade 2012. Ministry of Economy, Trade and Industry (Tokyo).

Notteboom, T., Haralambides, H., and Cullinane, K. (2024). The Red Sea crisis: Ramifications for vessel operations, shipping networks, and maritime supply chains. *Maritime Economics & Logistics*, 26(1):1–20.

Notteboom, T., Pallis, T., and Rodrigue, J.-P. (2021). Disruptions and resilience in global container shipping and ports: The COVID-19 pandemic versus the 2008-2009 financial crisis. *Maritime Economics & Logistics*, 2021(23):179–210.

Saxenian, A. (2004). Taiwan's Hsinchu region: Imitator and partner for Silicon Valley. In Bresnahan, T. and Gambardella, A., editors, *Building High-Tech Clusters: Silicon Valley and Beyond*, pages 190–228. Cambridge University Press, Cambridge.

Tran, N. K., Haralambides, H., Notteboom, T., and Cullinane, K. (2025). The costs of maritime supply chain disruptions: The case of the Suez Canal blockage by the 'Ever Given' megaship. *International Journal of Production Economics*, 279:109464.

UNISDR (2012). Reducing vulnerability and exposure to disasters: Asia-Pacific Disaster Report 2012. United Nations Office for Disaster Risk Reduction, Bangkok.